ISTANBUL TECHNICAL UNIVERSITY ★ EURASIA INSTITUTE OF EARTH SCIENCES

MOBILE CRATONS, SUBCRETION TECTONICS AND FORMATION OF TTGs

M.Sc. THESIS

Uğurcan ÇETİNER

Department of Solid Earth Sciences

Geodynamics Programme

Thesis Advisor: Assoc. Prof. Oğuz H. GÖĞÜŞ

JUNE 2019

ISTANBUL TECHNICAL UNIVERSITY ★ EURASIA INSTITUTE OF EARTH SCIENCES

MOBILE CRATONS, SUBCRETION TECTONICS AND FORMATION OF TTGs

M.Sc. THESIS

Uğurcan ÇETİNER

(602171003)

Department of Solid Earth Sciences

Geodynamics Programme

Thesis Advisor: Assoc. Prof. Oğuz H. GÖĞÜŞ

JUNE 2019

İSTANBUL TEKNİK ÜNİVERSİTESİ ★ AVRASYA YER BİLİMLERİ ENSTİTÜSÜ

MOBİL KRATONLAR, BİRİKME TEKTONİĞİ VE TTG'LERİN OLUŞUMU

YÜKSEK LİSANS TEZİ

Uğurcan ÇETİNER

(602171003)

Katı Yer Bilimleri Anabilim Dalı

Jeodinamik Programı

Tez Danışmanı: Doç. Dr. Oğuz H. GÖĞÜŞ

HAZİRAN 2019

Uğurcan Çetiner, a M.Sc. student of İTU Eurasia Institute of Earth Sciences student ID 602171003, successfully defended the thesis/dissertation entitled “MOBILE CRATONS, SUBCRETION TECTONICS AND FORMATION OF TTGs”, which he prepared after fulfilling the requirements specified in the associated legislations, before the jury whose signatures are below.

Thesis Advisor: **Assoc. Prof. Oğuz H. Göğüş** ……..................................
Istanbul Technical University

Jury Members: **Prof. Dr. Hans THYBO** ……..................................
Istanbul Technical University

Dr. Derya GÜRER ……..................................
The University of Queensland

Date of Submisson: 03.05.2019
Date of Defense: 10.06.2019

To my family,

FOREWORD

First, I would like to thank my thesis supervisor Assoc. Prof. Oğuz H. Göğüş for his continuous guidance, support and patience during my master’s education. I am very grateful to have agreed to work with her as bachelor and master student.

I am beholden to the institute manager Prof. Dr. Attila Çiner and other institute members for providing me an office at the university during my research and, I am grateful for their contributions.

I also would like to thank to Antoine Rozel for letting me use the convection code StagYY and, his invaluable time and effort to improve my research. I am also very grateful to him for his crucial contributions to my master thesis.

I would like to thank to my dear colleagues Açelya Ballı, Ömer Bodur and Barış Şen for helping me get through hard times during my research. I am grateful to Ceyhun Erman, Caner Memiş and Hacı Ahmet Gezgin for their invaluable supports.

Finally, I would like to thank to my parents Hasan Çetiner and Müjgan Çetiner and my sister Gizemnur Çetiner for their unrequited love and support to me during my whole life.

June 2019 Uğurcan ÇETİNER

TABLE OF CONTENTS

Page
FOREWORD .... **ix**
TABLE OF CONTENTS .... **xi**
ABBREVIATIONS .... **xiii**
SYMBOLS .... **xv**
LIST OF TABLES .... **xvii**
LIST OF FIGURES .... **xix**
SUMMARY .... **xxi**
ÖZET .... **xxiii**
1. INTRODUCTION **1**
  1.1 Former Studies and Plate Tectonics Problem in Archean 3
    1.1.1 Plate tectonics vs. stagnant-lid 3
    1.1.2 Formation of TTGs and cratonic mantle lithosphere 6
  1.2 Objectives 8
2. METHODS **11**
3. EXPERIMENTAL RESULTS & DISCUSSION **15**
  3.1 Reference Model (Experiment A1) 15
  3.2 Effects of Deformation Mechanism (Experiment A2) 19
  3.3 Effects of Surface Yield Stress (Experiments B1, B2 & B3) 24
    3.3.1 Experiment B1 25
    3.3.2 Experiment B2 28
    3.3.3 Experiment B3 32
  3.4 Effects of Eclogite Transition Depth (Experiment C1 & Experiment C2) 33
    3.4.1 Experiment C1 34
    3.4.2 Experiment C2 38
  3.5 Effects of Reference Mantle Viscosity (Experiment D1 & Experiment D2) 42
    3.5.1 Experiment D1 42
    3.5.2 Experiment D2 43
4. CONCLUSIONS **53**
REFERENCES **57**
CURRICULUM VITAE **63**

ABBREVIATIONS

Fo : Forsterite Ratio
Ga : Billion Years Ago
Ma : Million Years Ago
Myr : Million Years
OUZO : Overturn Upwelling Zone
RHP : Radioactive Heat Production
SCLM : Sub-continental Lithospheric Mantle
SOLM : Sub-Oceanic Lithospheric Mantle
TTG : Tonalite-Trondjemite-Granodiorite

SYMBOLS

κ : Thermal conductivity
τ : Shear stress
C : Cohesion
σ : Normal stress
g : Gravity vector
t : Time
u,v : Displacement Vector Components
T : Temperature
C_p : Heat capacity
H : Rate of internal heat production
α : Thermal expansion coefficient
ρ : Density
θ : Angle of friction
$\dot{\varepsilon}$: Strain rate
A : Viscosity parameter
n : Power exponent
Q : Activation energy
R : Ideal gas constant
Mg# : Magnesium number

LIST OF TABLES

Page

Table 1.1 : The onset of plate tectonics according to different studies (Modified after Arndt, 2013). **5**
Table 3.1: Model parameters for Experiment A1 .... **15**
Table 3.2 : Model Parameter for Experiment A2.......... **20**
Table 3.3 : Model parameters for Experiment B1.......... **25**
Table 3.4 : Model Parameters for Experiment B2 .... **29**
Table 3.5 : Model Parameters for Experiment B3 .... **32**
Table 3.6 : Model Parameters for Experiment C1. .... **34**
Table 3.7 : Model Parameters for Experiment C2. .... **38**
Table 3.8 : Model parameters for Experiment D1. .... **42**
Table 3.9 : Model Parameters for Experiment D2. .... **44**
Table 3.10 : Summarization of Experimental Results.......... **50**

LIST OF FIGURES

Page

Figure 1.1 : Ages of continental lithospheres around the world (Artemieva, 2011)... **1**
Figure 1.2 : a) Anorthite-Albite-Orthoclase triangle showing the K-rich modern granitic rocks (red area) and TTGs (green dots), b) K-Na-Ca triangle shows K-enrichment during the formation of continental granitoids (red). TTGs does not show a clear trend (modified after Moyen & Martin, 2012)... **2**
Figure 1.3 : Primitive mantle normalized spider diagram for trace elements of TTGs (green) and modern crustal rocks (red) (after Moyen & Martin, 2012). . **2**
Figure 1.4 : Overturn Upwelling Zones (Bédard, 2018). **7**
Figure 1.5 : Subcretion of oceanic lithosphere, and formation TTGs by the melting of eclogitic rocks (Modified after Bédard, 2018). **8**
Figure 2.1 : Reference model setup. **12**
Figure 2.2 : Geothermal gradients for oceanic (blue) and continental (orange) lithospheres.. **13**
Figure 3.1 : Craton becomes mobilized at t = 160.207 Myr. **16**
Figure 3.2 : A rift opens on the left side of the craton while some parts of oceanic lithosphere, located on the left and the right side of the craton, drifts away with the moving craton. **17**
Figure 3.3 : Hot asthenospheric rocks rises through the opening near the left boundary, and oceanic lithosphere becomes subcreted at the right margin of the craton. **18**
Figure 3.4 : Oceanic lithosphere gets compressed on the periodic boundary, gets thicker and eclogitizes. **19**
Figure 3.5 : Dislocation creep extends mobilization time around ~35 Myr. **21**
Figure 3.6 : Phase transition of the oceanic parts into eclogite creates an eclogitic drip on the right, and a rift opens on the left side where the oceanic crust became weaker and thinner **22**
Figure 3.7 : Oceanic lithosphere attached to the craton, subcretes and eclogitizes at the left margin. Another rift starts to open on the right side of the craton. Craton stalls (and even moves a bit backwards) due to direction of convecting cells. **23**
Figure 3.8 : Asthenospheric rocks rising from the rift located on the right, helps to the subcretion of oceanic lithosphere. **24**
Figure 3.9 : The craton starts to drift away at t = 207.436 Myr. **26**
Figure 3.10 : Thickened parts of oceanic lithosphere drips away, and a ridge forms on the left side of the craton **27**
Figure 3.11 : A drip along the periodic boundary forms due to craton push and counterclockwise convection cell... **28**
Figure 3.12 : Craton becomes mobilized ~150 Myr later from previous models. **30**

Figure 3.13 : Rifting on the left side results in generation of new oceanic crust. Meanwhile, oceanic lithosphere becomes thicker near the right boundary. **31**
Figure 3.14 : When surface yield stress is 40 MPa, craton does not drift away under given conditions.......... **33**
Figure 3.15 : Craton starts to drift away at t=136.035 Myr. **35**
Figure 3.16 : Eclogitic drip forming on the periodic boundary due to crustal thickening. **36**
Figure 3.17 : Subcreted basaltic oceanic crust becomes denser due to eclogitization and sinks as a viscous drip.......... **37**
Figure 3.18 : Asthenosphere rises through the rift formed on the left-hand side. Basaltic crustal material undergoes phase transition into eclogite and forms and eclogitic drip. **39**
Figure 3.19 : Oceanic lithosphere gets thicker on the right side due to compressional forces. **40**
Figure 3.20 : A secondary drip forms as craton pushes the buoyant lithosphere...... **41**
Figure 3.21 : Craton becomes wider and thinner in time, and undulation due to deformation of the oceanic lithosphere can be observed. **43**
Figure 3.22 : Craton becomes mobilized at t = 7.216 Myr. Asthenosphere rising through the rift drags oceanic lithosphere into the mantle. **45**
Figure 3.23 : First part of oceanic lithosphere that has been sinking breaks-off, while a second one starts to form out of newly formed oceanic crust. **46**
Figure 3.24 : Second slab breaks-off, a third one forms and starts to sink down as previous ones. **47**
Figure 3.25 : 1350 km displacement of the cratonic roots for each model. **48**
Figure 3.26 : Classification of different behaviors observed in the study, and corresponding experiments.......... **49**
Figure 4.1 : Comparison of different experiments with varying viscosities from this study and evolution of tectonic regime in the Archean according to Cawood et al. (2018). **54**

MOBILE CRATONS, SUBCRETION TECTONICS AND FORMATION OF TTGs

SUMMARY

The formation of Archean cratonic lithosphere and TTG (Tonalite-Trondjemite-Granodiorite) suites is not well understood, in part because the style of global tectonics active at that time is uncertain. The non-plate tectonic hypothesis for formation and evolution of continents we test in this study involves: intense magmatism above mantle upwellings in an unstable single plate regime to form cratonic nucleii; imbrication and anatexis of crust-dominated oceanic lithosphere at convergent margins driven by mantle flow, with build-up and thickening of cratonic keels by collisions. We use 2D numerical geodynamic models to investigate whether differential motion between the convecting mantle and cratonic keels can induce horizontal motion of a craton to form an accretionary orogen. Using the convection code StagYY, we attempt to model a self-consistent subcretion of oceanic lithosphere pushed by a pre-imposed craton. Initially, 40 km thick basaltic crust, accompanied by 20 km thick sub-oceanic lithosphere, is introduced on both sides of the 230 km thick cratonic lithosphere, with an initial potential mantle temperature of 1750 K. The domain is divided by 64 vertical cells and 512 lateral cells corresponding to 660 km depth and 2000 km length. Both for upper and lower boundary, free-slip surface conditions are used. Left and right boundaries are periodic. Velocities are forced to be zero until a critical depth of 60 km, after that, a sub-lithospheric mantle flow of 4 cm/yr imposed into the model. Diffusion creep has chosen to be the main deformation mechanism for computational reasons. Our study involves investigating the effects of different parameters on the evolution of the experiments, such as; reference mantle viscosity, eclogite phase transition depth, yield stress of the oceanic lithopshere, and a change in the deformation mechanism. Our experimental results indicate that, cratonic keels can be mobilized by the sub-lithospheric mantle winds. We chose a reference model with typical yield stress (20 MPa), mantle viscosity (10^{20} Pa s), and eclogite transition depth (40 km) values, where craton becomes mobilized after ~160 Myr from model initiation, and oceanic lithosphere becomes subcreted at the cratonic margin. It has been found that, reference mantle viscosity has a significant impact on the exact time that the craton has become mobilized. Experiments with a 10^{21} Pa s reference mantle viscosity yielded in faster mobilizaiton times by a factor 22 – 23 times. In these models, subcretion of oceanic lithosphere at continental margins did not occur, but thickened oceanic lithosphere parts created downwellings resembling to subducting oceanic slabs. Lower mantle viscosities (10^{19} Pa s), however, could not generate sufficient stress to drift the craton away, but they led to a more vigorous convection and thermally eroded the cratonic roots. Increasing yield stresses from 20 MPa to 25 MPa and 30 MPa, made the oceanic lithosphere stronger and elongated the time needed for cratonic mobilization. Increasing it to 40 MPa led to a stable tectonic state, where craton did not become mobilized. Experiments with increased surface yield stresses did not provide an environment for subcretion tectonics, instead, lithospheric removal was due to eclogitic dripping where oceanic lithosphere became thick enough. Removal of the oceanic lithosphere changes velocity and orientation of the flows within the asthenosphere. In relation to that, evolution of some experiments contained convection cells generated within the mantle that ceased the motion of the craton, and even pushed it backwards for brief amount of time in some cases. Experiment performed to investigate the effect of deformation mechanism reflected the best example for this. In this case, rigthward moving craton traveled backwards at some point, created a subcretion on the left margin, and then, it started to move forward again to create a secondary subcretion, which has been classified as asynchronous double-sided subcretion. Our results indicate that, lithospheric removal mechanisms and craton mobilization times can vary with different parameters, but a displacement of 1350 km takes place in 30 to 40 Myr in all experiments, when the craton becomes mobile. Subcretion tectonics can only start in a narrow window, where surface yield stress is 20 MPa and reference mantle viscosity is 10^{20} Pa s, with the exception of eclogite transition depth being 60 km. Results indicate that subcretion mechanism can be achieved under given conditions, and TTG genesis via this mechanism can be valid when certain P-T conditions are met.

MOBİL KRATONLAR, BİRİKME TEKTONİĞİ VE TTG OLUŞUMU

ÖZET

Günümüz kıtalarının ataları olarak kabul edilebilecek Arkeen dönemi kratonik litosferinin, ve TTG (Tonalit-Tronjemit-Granodiyorit) kayalarının oluşumu, o dönemdeki tektonik rejim iyi bilinmediğinden net olarak anlaşılamamıştır. Dünya kıtasal kabuğunun yaklaşık %16'sı Arkeen yaşlıdır. Ayrıca, Arkeen kratonların manto litosferleri oldukça tükenmiş materyalden oluşurlar ve buna bağlı olarak yüzebilirlikleri yüksek olduğundan uzun dönemler boyunca duraylı kalabilme özelliğine sahiptirler. Arkeen yaşlı kıta kabuğunun çoğunluğu Tonalit-Tronjemit-Granodiyorit (TTG) serisi kayalarından oluşmaktadır. Bu tip kayaların SiO_2 içerikleri çoğunlukla %70'den büyük olmakla birlikte, günümüz granitik kayalarıyla kıyaslandığında yüksek Na_2O ve düşük K_2O içerikleri ile karakterize olurlar. İz element desenlerinde görülen negatif Nb ve Ta anomalisi bu kayaların kıta içi bölgelerdense, orojenik ortamlarda oluştuklarını işaret etmektedir. TTG tipi kayaların kimyasal özellikleri yapılan çalışmalar ile sınırlandırılmış olsa da, levha tektoniğinin nasıl ve ne zaman başladığının kesin olarak bilinmemesi, oluştukları tektonik rejim ve ortam açısından farklı yorumlara sebebiyet vermektedir. Bu nedenle dünyanın tektonik olarak ölü halde kabul edilebilecek tek plakalı bir rejimden nasıl levha tektoniğine geçtiğini anlamak, TTG oluşumu tartışmalarına da açıklık getirebilir. Arkeen yaşlı ultra yüksek basınç kayalarının (mavi şist), ofiyolitlerin ve yatay sıkışma bölgelerinde olması beklenen bindirme fayları ile kıvrımlanmaların yokluğu; bu dönemde levha tektoniğinin olmadığı öngörüsünü güçlendirmektedir. Bu çalışmada test edilen levha tektoniği olmayan dünya teorisi; duraysız, tek plakalı bir dünyada, manto yükselmeleri dolayısıyla açığa çıkan yoğun magmatizmanın kratonik çekirdekleri oluşturması ve çoğunluğu okyanusal kabuktan oluşan okyanusal litosferin, manto akışları tarafından tetiklenmiş hareketi sonucu bindirme ve anaergimesiyle kratonik kökleri kalınlaştırıp güçlendirmesi üzerinde durmaktadır. 2-boyutlu jeodinamik modeller kullanılarak, konveksiyon halindeki manto ve kratonik kökler arasındaki diferansiyel hareketin, kratonu hareket ettirerek akresyonel bir orojen oluşturup oluşturamayacağı incelenmiştir. Çalışmada kullanılan StagYY konveksiyon kodu ile, model içerisine yerleştirilmiş bir kratonun okyanusal kabuğu ittirmesi sonucu istikrarlı bir birikim ve yığışım hareketinin modellenmesi amaçlanmıştır. Model başlangıcında, potansiyel manto sıcaklığı 1750 K olacak şekilde; 230 km kalınlığında bir kraton ve, kratonun sağ ve sol kısmında ona eşlik eden 20 km'lik okyanusal manto litosferiyle birlikte 40 km'lik okyanusal bazaltik kabuk yerleştirilmiştir. Üst ve alt sınır için serbest kayma sınır koşulu kullanılmıştır. Sağ ve sol sınırlar ise periyodiktir. Periyodik sınır koşullarında bir sınırdan çıkan materyal diğer kısımdan girdiğinden, içeri akan yeni materyalin fiziksel ve kimyasal özelliklerinin kontrol edilmesi gerekmemektedir. Hızlar 60 km'lik bir kritik derinliğe kadar 0 olmaya zorlanmış, bu derinlikten sonra 4 cm/yıl'lık litosfer altı manto akış hızları kullanılmıştır. Bilgisayar sayısal işlem sorunları dolayısıyla, ana deformasyon

mekanizması olarak yayınımlı sürünme (Newtonsal akış) tercih edilmiştir. Çalışma; referans manto viskozitesi, eklojit faz dönüşüm derinliği, okyanusal litosferin sünme gerilmesi ve deformasyon mekanizmasındaki değişimlerin etkisinin incelenmesini içermektedir. Deneysel sonuçlar, kratonik gövdelerin litosfer altı manto rüzgarları yardımıyla hareket ettirilebileceğini göstermiştir. Kratonun model başlangıcından 160 milyon yıl sonra mobil hale geçtiği, okyanusal litosferin kraton kenarında biriktiği ve, sünme gerilimi (20 MPa), manto viskozitesi (10^{20} Pa s) ve eklojit dönüşüm derinliği (40 km) için tipik değerlerin kullanıldığı deney, referans model olarak seçilmiştir. Devamında, referans manto viskozitesinin kraton mobil hale geçme zamanında önemli bir rol oynadığı tespit edilmiştir. 10^{21} Pa s referans manto viskozitesine sahip modellerde mobilleşmenin 22-23 kat daha hızlı gerçekleştiği tespit edilmiştir. Bu modellerde okyanusal litosferin kıta kenarında birikmesi gerçekleşmemiştir ancak, okyanusal litosferin kalınlaşan kesimlerinde yiten okyanusal levhalara benzeyen parçaların aşağı yönlü hareketi gözlenmiştir. Daha düşük manto viskozitesinin (10^{19} Pa s) kullanıldığı modellerde ise, kratonu hareket ettirecek yeterli streslere ulaşılamamış, ancak, manto içerisinde oluşan kuvvetli akışlar sonucu kratonik köklerin termal erozyonu gerçekleşmiştir. Viskozite artışı kratonun harekete başlayışını hızlandırsa da, toplam hareket süresini önemli ölçüde etkilememektedir. Modellerin tümünden alınan sonuçlara göre, manto akışları sayesinde harekete başlayan kratonlar model kutusunun bir sınırından diğer sınırına olan yatay hareketini 30 – 40 milyon yılda tamamlamaktadır. Sünme gerilimini 20 MPa'dan 25 MPa ve daha sonra 30 MPa'a çıkarıldığı modellerde okyanusal litosferin güçlenmesi sonucu kraton harekete geçme süresinin uzadığı gözlenmiştir. 40 MPa'a çıkarıldığı durumda ise kraton stabil bir tektonik durumda kalmış ve hareket etmemiştir. Sünme gerilmesinin artırıldığı modellerde birikmeli tektonik gözlenmemiş onun yerine, okyanusal litosferin kalınlaştığı yerlerde gözlenen eklojitik manto damlamaları oluşmuştur. Sünme gerilimindeki göreceli olarak küçük (5-10 MPa) değişikliklerin model evriminde tektonik açıdan önemli değişiklikler yaratmış olması, sünme gerilimi değerinin farklı tektonik rejimler arasında keskin bir geçiş olduğunu göstermektedir. Okyanusal litosferin bir şekilde astenosferin içerisine taşınması, manto içerisindeki akışların hızını ve yönünü etkileyebilmektedir. Buna bağlı olarak bazı modellerin evrimi süresince açığa çıkan konveksiyon hücreleri kratonun hareketini durdurmuş ve hatta bazı modellerde kısıtlı bir süre boyunca kratonu geriye doğru sürüklemiştir. Deformasyon mekanizmasının etkisini inceleyen model, bu durumun en güzel örneğini ortaya koymuştur. Bu durumda sağ yönde hareket eden kraton bir noktada ters yöne hareket etmeye başlayarak okyanusal litosferi kıta kenarında biriktirmiş, ve devamında kesilen sağ yönlü hareketini sürdürmesiyle sağ kısımdaki okyanusal litosferi biriktirmiştir. Bu durum eş zamanlı olmayan çift taraflı birikme adı verilmiştir. Sonuçlara göre, farklı parametreler altında litosfer taşınma tiplerinin ve kraton mobilleşme sürelerinin değiştiği gözlemlense de, kratonik gövdelerin harekete başladıktan sonra yaptıkları 1350 km'lik yer değiştirmenin 30 ila 40 milyon yıl arasında gerçekleştiği tespit edilmiştir. Eklojit faz dönüşümü derinliğinin 60 km olduğu model istisnai olmakla birlikte, birikme tektoniğinin; sünme gerilmesinin 20 MPa ve referans manto viskozitesinin 10^{20} Pa s olduğu dar bir aralıkta gerçekleştiği tespit edilmiştir. Model sonuçları, artan viskozitenin model evrimi süresince gözlenen tektonik rejimlerde değişime yol açtığını göstermektedir. Düşük viskoziteden yüksek viskoziteye doğru artış esnasında tek plakalı bir rejimden levha tektoniğine geçişe benzeyen bir geçişin söz konusu olduğu tespit edilmiştir. Modellerdeki viskozite artışı, mantonun soğumasına bağlı olarak gerçekleşen viskozite artışıyla ilişkilendirilebileceğinden, nümerik deneyler tek plakalı rejimden levha tektoniğine geçişin viskoziteyle bağlantılı olabileceğini göstermektedir. Uygun olduğu belirlenen parametreler altında, gerekli sıcaklık-basınç koşulları sağlanması kaydıyla, birikme tektoniği TTG'lerin oluşmasına sebep olabilir.

1. INTRODUCTION

Descendants of the oldest continental pieces, cratons, are the foundation of modern-day continents. They are the most stable and least deformed places on the Earth. Their deep, depleted and stable roots combined with their uncommon crustal lithology and their economic significance because of the diamond-bearing kimberlite pipes, makes them a conspicuous study case in earth sciences. (Groves et al., 1987; Shirey et al., 2004).

Roughly 16% of the Earth’s continental crust is composed of rocks that are Archean in age (Artemieva, 2011). Mantle lithosphere of Archean cratons are made up by highly depleted material, which makes them neutrally buoyant and stable for very long time (Jordan, 1978). Roots of these peculiar structures can reach down into the mantle about 200-300 km deep (King, 2005; Wen & Anderson, 1997).

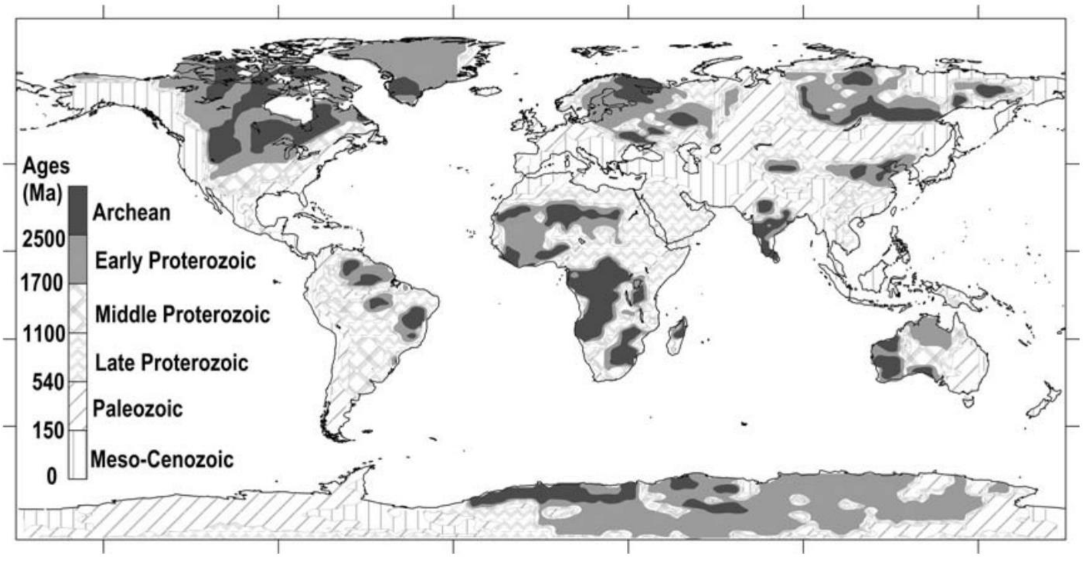

Figure 1.1 : Ages of continental lithospheres around the world (Artemieva, 2011).

Archean age continental crust mainly consists of TTGs, a series of rocks which mostly have 70% or more SiO_2 content. They are characterized by high Na_2O content (3.0-7.0 wt% Na_2O) and low K_2O/Na_2O ratio (<0.5). They have relatively low potassium content when compared with modern granitic rocks. Generation of modern granitoids shows a differentiation during potassium enrichment, while TTGs do not follow a trend (Figure 1.2).

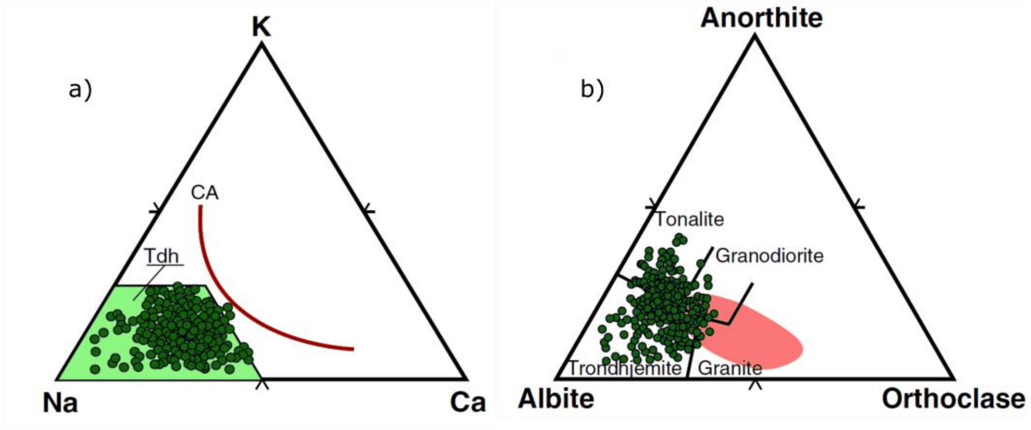

Figure 1.2 : a) Anorthite-Albite-Orthoclase triangle showing the K-rich modern granitic rocks (red area) and TTGs (green dots), b) K-Na-Ca triangle shows K-enrichment during the formation of continental granitoids (red). TTGs does not show a clear trend (modified after Moyen & Martin, 2012)

Major minerals in the rock; quartz, oligoclase and biotite are accompanied by the accessory minerals allanite, apatite, zircon, titanite and titanomagnetite. They have an average Mg# of 43, which leads to conclusion that they are poor in ferromagnesian components (Moyen & Martin, 2012).

They are more enriched in LREE compared with the modern granitoids. Both TTGs and new generation of granitic rocks have negative Nb and Ta anomalies, indicating that they should have been formed in an orogenic environment rather than intra-plate regions (Figure 1.3) (Kelemen et al., 1998).

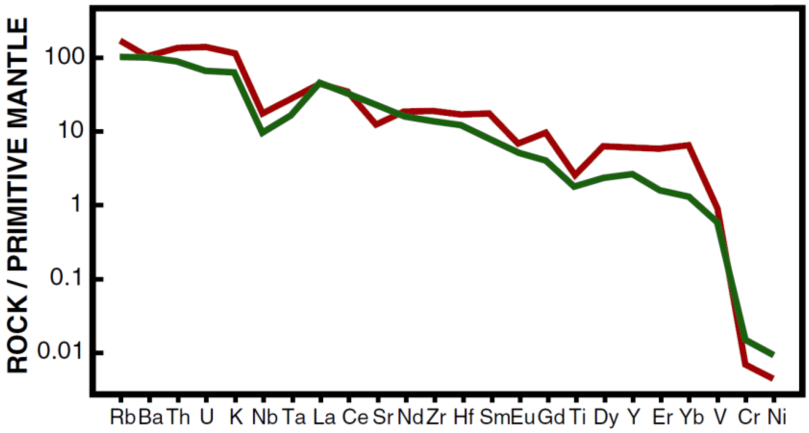

Figure 1.3 : Primitive mantle normalized spider diagram for trace elements of TTGs (green) and modern crustal rocks (red) (after Moyen & Martin, 2012).

According to Moyen and Martin (2012), most accepted model for the formation of TTG parental magmas starts with partial melting of mantle material to generate basalts. These basalts then experience eclogitization under the suitable P-T conditions, which can give rise to generation of tonalitic magmas, if partially melted. Differentiation of the tonalitic magmas with the extraction of hornblende ± plagioclase might have affected some suites, leading to the genesis of different types of more evolved TTG magmas (Martin, 1987; Moyen et al., 2007).

Archean aged subcontinental lithospheric mantles (SCLM) are highly viscous, Fe-depleted, refractory and buoyant. They are the most stable regions in Earth with no or little internal deformation (Aulbach et al., 2011; Bédard, 2006; Griffin et al., 2009) . Dominant mineral of the Archean SCLM is olivine, which has an unusual composition compared with its modern-day counterparts, has uncommonly high MgO/(MgO+FeO) ratios (Fo_{92-94}). This type of magnesian olivine cannot be produced with the modern-day mantle temperatures, thus, mantle temperatures should have been higher (~150 - 250 ^{0}C) in Archean (Arndt et al., 2009; Sizova et al., 2015). Starting from this point, formation of this unusual minerals require at least one of the followings: melting under extremely hot conditions, transformation of the less magnesian olivine into forsterite-rich olivine under the influence of tectonic events, separation of forsterite-rich olivine from its opposite by some physical process (Arndt et al, 2009).

(Lenardic & Moresi, 1999) suggested that, buoyancy by itself cannot be the only reason for the extreme durability of the cratons. Instead, combination of buoyancy and absence of volatiles in magnesian minerals (olivine and orthopyroxene) in the cratonic roots can lead to long-term stability of the cratons.

1.1 Former Studies and Plate Tectonics Problem in Archean

1.1.1 Plate tectonics vs. stagnant-lid

Formation mechanism for the Archean terrane is not well understood, in part because the global tectonic regime active that time is uncertain. In relation to this particular problem, scientists working on the topic are divided into two groups. First group of workers claims that, there was no subduction in Archean because, there is not enough compelling evidence for Archean aged ophiolites and ultra-high pressure metamorphic rocks (blueschists) (Bédard, 2006, 2018; Stern, 2008). While the advocates of plate tectonics state that, Archean crust cannot be formed without subduction, and remnants of Archean aged arc-type magmatism, thrust and isoclinal folds, and accretionary complexes are solid evidences for subduction (Smithies et al., 2005; van Kranendonk, 2011).

Stagnant-lid defines a state that can be considered as tectonically dead. It forms on top of a convective layer which is temperature dependent, and has a viscosity that is at least 10^4 less viscous than the overlying lid (Breuer, 2011). As a result, defining tectonic settings that comprise a type of deformation (i.e. rifts and/or gravitational downwellings and/or upwellings) needed new names such as, “heat-pipe regime” (Moore & Webb, 2013), “plutonic squishy lid” (Rozel et al., 2017), “plume-lid” (Fischer & Gerya, 2016), and “sluggish-lid” (O’Neill & Roberts, 2018). All these names, even though they differ in numerous ways from each other, refers to a single plate regime. Timing of transition from single plate to modern day plate tectonics is a subtopic of the Archean plate tectonics controversy. It is still a highly debated subject, and different studies suggest different evidences for initiation of subduction. A compilation of times suggested for the onset of plate tectonics is given in Table 1.1.

Stern (2018) suggests that, in order to have plate tectonics, lithosphere must be denser than the asthenosphere, parts of lithosphere must be rheologically strong enough to stay in one piece without breaking (i.e. so it can pull down the rest of the lithosphere sufficiently), and it must also contain rheologically weak zones so rifts and ridges can form to break continental pieces. He states that, all these conditions have not been met until the Neoprotorezoic due to absence of petrotectonic clues. Furthermore, it is well documented that, potential mantle temperatures in Archean must have been 150 – 200 ^{o}C higher than modern day mantle temperatures (Condie et al., 2016; Herzberg et al., 2010). Under these conditions, mantle lithosphere was probably thinner, rheologically weaker, and more buoyant. Even if there was subduction in Archean, it was probably episodic and short-lived (Sizova et al., 2015; Ueda et al., 2008). Arndt (2013) argues that, plate tectonics started as early as 4.0 Ga and subduction zones are the only candidate that can generate Archean crustal rocks.

Table 1.1 : The onset of plate tectonics according to different studies (Modified after Arndt, 2013).

When did plate tectonics start?	Studies	Evidence
~800 Ma	(Hamilton, 1998, 2011), (Stern, 2008, 2018)	Absence of lawsonite-bearing metamorphic rocks, blueschists, ophiolites and glaucophane-bearing eclogites.
1.8 – 2.7 Ga	(Brown, 2007), (Bédard, 2006, 2018; Bédard et al., 2003) (Rollinson, 2010)	Absence of thrust and fold belts, blueschists, flysch and molasse deposits, and mélanges.
2.7 Ga or Before	(van Hunen & Moyen, 2012), (Moyen & Martin, 2012), (Condie & Kröner, 2008)	Existence of Archean aged arc or arc-like compositions (boninites), lateral accretion on Archean provinces, high-pressure metamorphic rocks.
3.0 Ga	(Cawood et al., 2006), (Polat, 2012), (Condie & Benn, 2013)	
3.3 – 3.5 Ga	(van Kranendonk, 2007, 2011), (Smithies et al., 2007), (Zegers and Keken, 2001)	Radical change in the composition of sub-continental mantle lithosphere ~3 Ga, and eclogite inclusions found in diamonds.
4.0 - 4.3 Ga	(Harrison et al., 2008), (Nicholas T Arndt, 2013),(Hastie & Fitton, 2019)	Evidence for recycling of crust into the mantle from isotopic and trace element data acquired from Archean aged zircon grains.

1.1.2 Formation of TTGs and cratonic mantle lithosphere

Different interpretations of structural, compositional and isotopical evidences mentioned in the previous chapter, gave birth to various hypotheses that are trying to explain the craton formation, generally fall into three categories: (i) wide range of volcanism above an extremely hot plume activity (Arndt et al., 2009; Gerya, 2014; Lee, 2006), (ii) repetitive imbrication of oceanic lithosphere at convergent boundaries (Helmsteadt & Schulze, 1989; van Kranendonk, 2011), and (iii) thickening of cratonic keels with continental collision (Cooper et al., 2006; Gray & Pysklywec, 2012).

Volcanism generated by hot plume impingement hypothesis advocates, high degrees of polybaric melting can lead to formation of forsterite-rich olivine closer to base of the plume, while more fertile peridotitic rocks are located at the margins (Lee, 2006). Magnesian part of this isopycnic area forms the depleted SCLM, whilst Fe-bearing, fertile parts at the margins gets ejected because of the gravitational instability (Arndt et al., 2009).

Imbrication of oceanic lithosphere at arc-like environments based on the idea of stacking of oceanic lithosphere under continents with low-angle lateral tectonic movements. The hypothesis suggests that the accretion of subducting slabs, which are mostly formed by low-pressure peridotite provides explanation for the presence of thick, low-pressure origin of SCLM peridotites (Arndt et al., 2009; Gerya, 2014).

Thickening of cratonic keels by the thrust stacking is claimed to be the reason for the stability of the cratons due to increasing yield strength (Gerya, 2014). Gray & Pysklywec (2012) performed a series of numerical experiments to test the viability of collisional scenario under the Neoarchean conditions. They classified three different styles of deformation based on varying rheology and radioactive heat production (RHP): (a) imbrication, (b) pure-shear thickening and (c) underplating. They stated that, when lower crust is rheologically weak and RHP is sufficiently low, deformation is due to imbrication, while pure-shear thickening arises from high RHP and low-degree of coupling between lower crust and the mantle lithosphere. In the case where lower crust is rheologically strong, high degree of coupling between the crust and mantle lithosphere prevents the imbrication and/or shear thickening and leads to underplating.

Another mechanism suggested for the formation of Archean cratons is based upon the idea of mantle overturns. Bédard (2018), suggested that the Earth was in a single plate regime in the Archean. This single plate regime restricted the efficient cooling of the Earth to upper mantle. Small-scaled, unstable thermal convection cells located at the upper mantle prevented the formation of a thick sub-oceanic lithospheric mantle (SOLM), while heat coming from the core and radioactive heat production in the mantle, accumulated and generated a large-scale thermal upwelling, “Overturn Upwelling Zone (OUZO)”, rising from core-mantle boundary to surface (Figure 1.4).

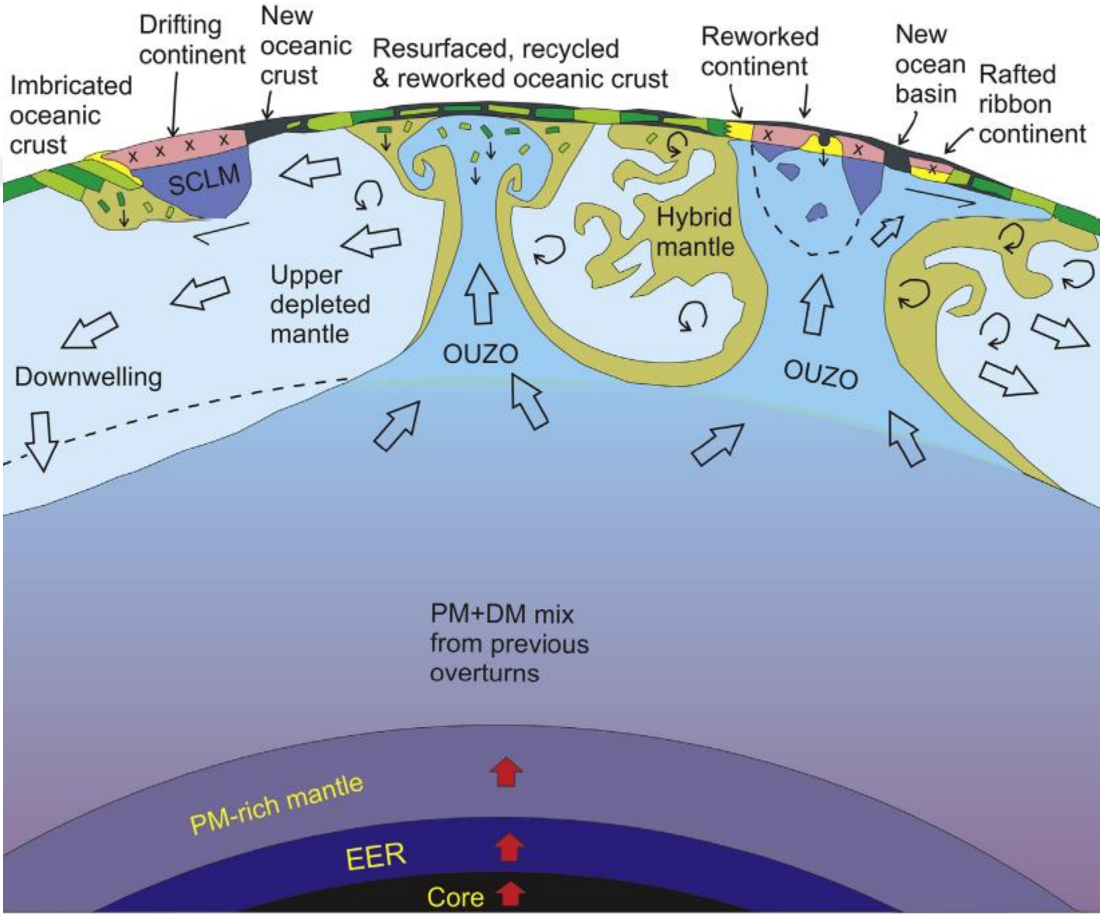
Imbricated oceanic crust
Drifting continent
New oceanic crust
Resurfaced, recycled & reworked oceanic crust
Reworked continent
New ocean basin
Rafted ribbon continent
SCLM
Hybrid mantle
Upper depleted mantle
Downwelling
OUZO
OUZO
PM+DM mix from previous overturns
PM-rich mantle
EER
Core

Figure 1.4 : Overturn Upwelling Zones (Bédard, 2018).

OUZO creates a traction in the sub-lithospheric mantle as it rises and, leads to the mobilization of distant continents/cratons. If OUZO encounters with a pre-existent continent, it recycles and reworks it. Continents mobilized by the traction starts to subcrete oceanic lithosphere at the margins. Thermal erosion created by the convection cells prevents the formation of a thick negatively buoyant sub-oceanic lithospheric mantle beneath the oceanic crust. Hence, unsubductable oceanic lithosphere thickens by subcretion at the continental margin. Subcreted basaltic oceanic crust metamorphose into eclogite as it sinks down, because of forces created by moving continent. Partial melting of these eclogitic parts form the TTG parental magmas (Figure 1.5).

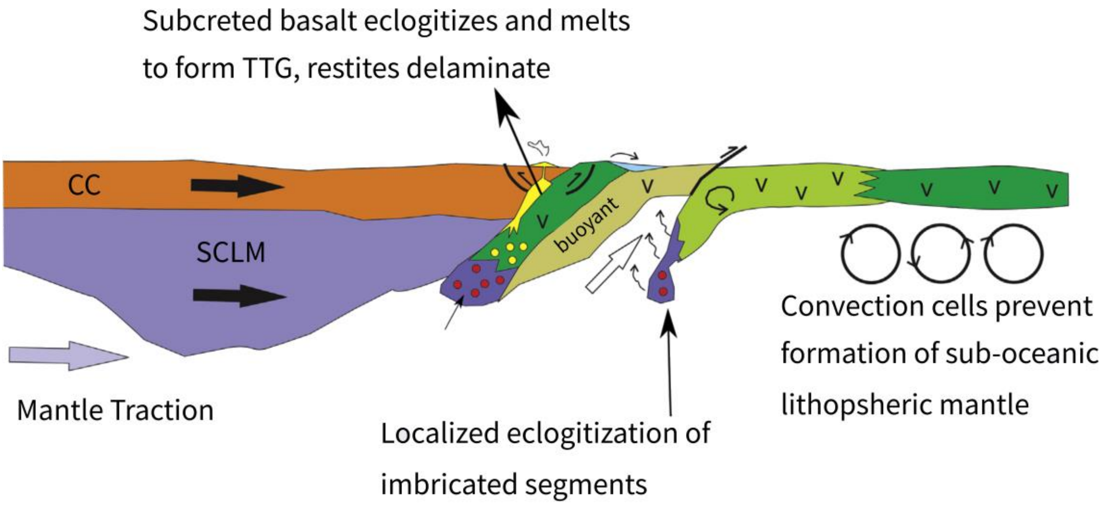
Subcreted basalt eclogitizes and melts to form TTG, restites delaminate
CC
SCLM
buoyant
V
Mantle Traction
Localized eclogitization of imbricated segments
Convection cells prevent formation of sub-oceanic lithopsheric mantle

Figure 1.5 : Subcretion of oceanic lithosphere, and formation TTGs by the melting of eclogitic rocks (Modified after Bédard, 2018).

1.2 Objectives

Main focus of our study is to bring an approach for understanding an Archean tectonic setting, where plate tectonics considered inactive. Volume of crustal rocks that have formed in the Archean should have been extensive due to higher mantle temperature, yet, the amount that has been preserved is lower than expected

(Johnson et al., 2014). In addition to this, TTGs, which comprise half to two-thirds of the crustal rocks which are formed in the Archean, are thought to be formed by a hydrated basaltic source. This indicates that there must be a form of crustal recycling even though there was no plate tectonics.

Objectives we are trying to accomplish in this study can be summarized as:

1) Achieve the mobilization of the cratons with stresses applied by the sub-lithospheric mantle winds on the cratonic keels,
2) Testing the effects of different reference mantle viscosities, eclogite phase transition depths, and surface yield stresses to the mobilization of cratons.

3) Testing the viability of subcretion of basaltic oceanic lithosphere at the continent-ocean borders,
4) Classifying the geodynamic regimes that have been identified within the parameter sweep, which can lead to crustal recycling under Archean conditions,

10

2. METHODS

Numerical experiments performed with convection code StagYY. It is a compressible code allowing parallelisation. It includes phase transitions, compositional variations, non-newtonian rheology and a set of different types of 2D and 3D geometries (Tackley, 2008). Conservation of mass, moment and energy are given, respectively;

$$\nabla.(\rho u) = 0 \tag{2.1}$$

$$-\nabla\big(2\eta\varepsilon(u)\big) + \nabla P = \rho(T)g \tag{2.2}$$

$$\frac{\partial T}{\partial t} + u\nabla T - \nabla(\kappa\nabla T) = \gamma \tag{2.3}$$

will be handled by the MUMPS solver within the PETSc package (Rozel et al., 2017), where, u is the fluid velocity, P is pressure (Pa), T is temperature (K), η is viscosity of the material (Pa s) and ε is rate of deformation (1/s). The parameters κ, γ, and g are the thermal conductivity (m^2 s^{-1}), thermal expansion coefficient (1/K), and gravity vector (m s^{-1}).

Petrological components of the mantle are 25% basalt and 75% harzburgite. It consists of 60% olivine and 40% pyroxene-garnet. The code has phase transitions at 410-520 km (Olivine-Wadsleyite) and 520-660 km (Wadsleyite-Ringwoodite) depth; while eclogite transformation of the basaltic crust starts 40-60 km depth. On the upper part of the eclogitization zone, olivine is 160 kg m^{-3} denser than basalt. Beneath the eclogite transformation zone, eclogite originated from basaltic source becomes 190 kg m^{-3} denser than olivine (Lourenço et al., 2016; Rozel et al., 2017).

Box geometry used for the model domain is divided into 64 vertical and 512 lateral cells, corresponding to 660 km in depth and 2000 km in length. Both for the upper and lower boundary, free-slip boundary conditions have been used. Left and right boundaries of the box have periodic boundary conditions. Initial model geometry comprises a 230 km thick cratonic keel (Rolf & Tackley, 2011), surrounded by 40 km thick basaltic crust accompanied by 20 km thick oceanic mantle lithosphere (Bédard, 2018). Center of the craton located at x = 500 km, and uppermost part of the craton is 300 km wide. A sub-lithospheric mantle flow of 4 cm/yr is imposed in the model to create mantle traction. Velocities are forced to be zero from surface to a critical depth of 60 km. A rift on the left and a thermal anomaly on the right side of the craton were implemented. The rift on the left margin of the craton is needed to imitate the separation between oceanic lithosphere and the craton on the left margin, which is thought to be a result of mobilization of a cratonic keel (Bédard, 2018). Thermal anomaly is to help localize the deformation (Figure 2.1).

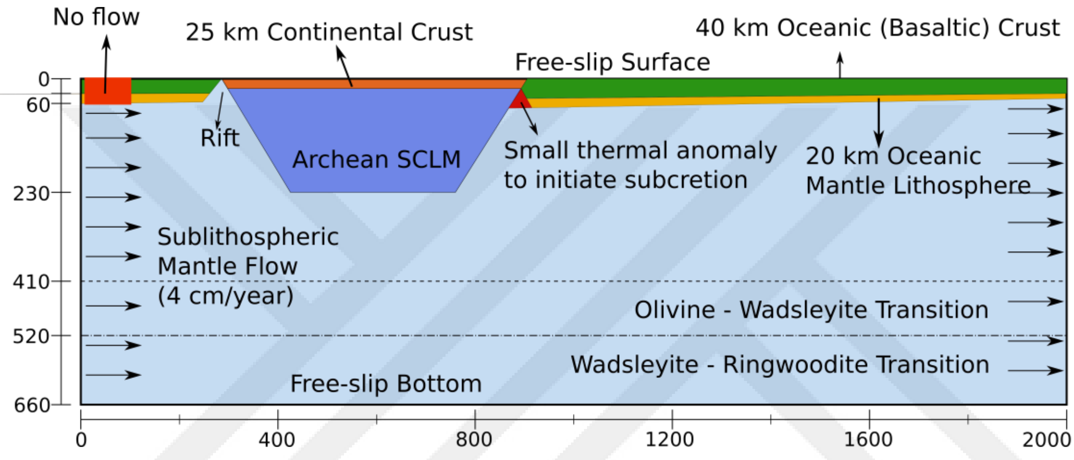
No flow
25 km Continental Crust
40 km Oceanic (Basaltic) Crust
Free-slip Surface
0
60
230
410
520
660
Rift
Archean SCLM
Small thermal anomaly
to initiate subcretion
20 km Oceanic
Mantle Lithosphere
Sublithospheric
Mantle Flow
(4 cm/year)
Olivine - Wadsleyite Transition
Wadsleyite - Ringwoodite Transition
Free-slip Bottom
0
400
800
1200
1600
2000

Figure 2.1 : Reference model setup.

Viscosity is considered temperature and depth (pressure) dependent, following Arrhenius Law:

$$\eta_{diff}(T,P) = \eta_0 \Delta\eta_i exp\left(\frac{(E_i + PV_i)}{RT} - \frac{E_i}{RT_0}\right) \tag{2.4}$$

where, η_0 is the reference mantle viscosity (10^{21} Pa s) at zero pressure and reference temperature T_0. $\Delta\eta_i$ is the factor used for viscosity jumps between layers. E_i is the activation energy in layer i, P is the pressure, V_i is the activation volume, R is the gas constant (8.314 J mol^{-1} K^{-1}), and the T is the absolute temperature (Rozel et al., 2017). The cratonic root is 200 times more viscous than the surrounding mantle, while the continental crust emplaced over the cratonic root is 10 times more viscous than the mantle. Standard visco-plastic approach has been used to perform yielding. Yield stress calculations have both brittle and ductile components;

$$\sigma_{brittle} = c + fP \tag{2.5}$$

$$\sigma_{ductile} = \tau_y + P\tau_y' \tag{2.6}$$

where c is cohesion (Pa), f is the friction coefficient, τ_y is the yield stress (Pa), τ_y' is the yield stress gradient, and f is the friction coefficient.

Yield stress gradient is set to a low value (0.005) to efficiently yield the lithosphere. Even though, it has no physical meaning, it is needed in the geodynamic models to yield the lithosphere and generate downwellings. The yield stress is increased for the cratonic root to prevent deformation. 1.2 GPa yield stress has been used for the craton while the yield stress gradient is same as elsewhere (0.005).

In the mantle, an adiabatic temperature profile has been used, starting at a surface potential temperature of 1750 K (i.e., about 150 K warmer than present day value). The surface temperature is 300 K, while the bottom boundary fixed at 2100 K (Figure 2.2).

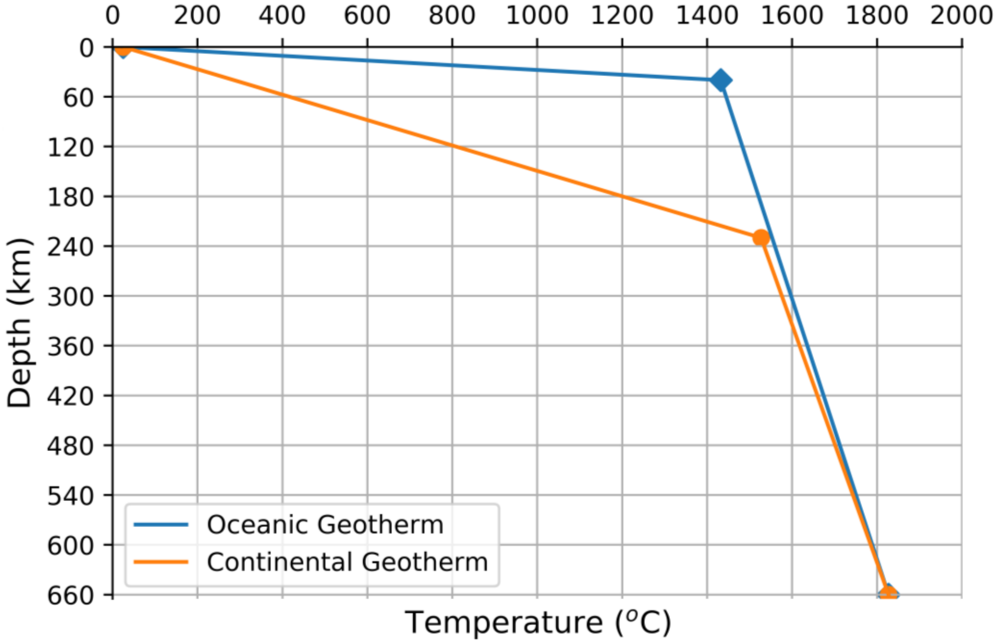

Figure 2.2 : Geothermal gradients for oceanic (blue) and continental (orange) lithospheres

3. EXPERIMENTAL RESULTS & DISCUSSION

3.1 Reference Model (Experiment A1)

Experiment A1 has chosen to be reference model due to its consistency with the proposed subcretion mechanism. In this model a cratonic root with 300 km radius had imposed into the model with a sub-lithospheric mantle flow of 4 cm/yr. Surface yield stress is 20 MPa while reference mantle viscosity is 10^{20} Pa s. Deformation depends on diffusion creep and there is no grain size evolution throughout the model. Eclogitization of basaltic crust starts at a depth of 40 km. All other model parameters are given in Table 3.1.

Table 3.1 : Model parameters for Experiment A1

Experiment # A1		
Reference Mantle Viscosity	10^{20}	Pa s
Surface Yield Stress	20	MPa
Friction Coefficient	0.1	
Thermal Anomaly Size	0.5	
Eclogite Phase Transition Depth	40	km
Cohesion	10^{3}	Pa
Deformation Mechanism	Diffusion	
Continent Radius (km)	300	km
Mantle Flow Velocity	4	cm/yr
Mantle Flow Starting Depth	60	km

In this experiment, cratonic keel becomes mobilized at 160.207 Myr (Figure 3.1). After craton starts to drift away, asthenosphere rises to the surface from the left side of the craton. This leads to formation of a structure resembling to mid-ocean ridges. Rising asthenosphere leads to thickening of the oceanic lithosphere on the left-hand side, basaltic oceanic crust turns into eclogite, gets denser and starts to sink. While the denser parts are sinking, they pull down left of the basaltic oceanic crust, just like slab-pull forces that are acting on modern-day subduction systems. An eroded part of the cratonic root can also be seen as viscous dripping. Oceanic lithosphere covers the both side of the craton. A structure resembling to a mid-ocean ridge forms on the right side of the craton, which mantle material rises through (Figure 3.2).

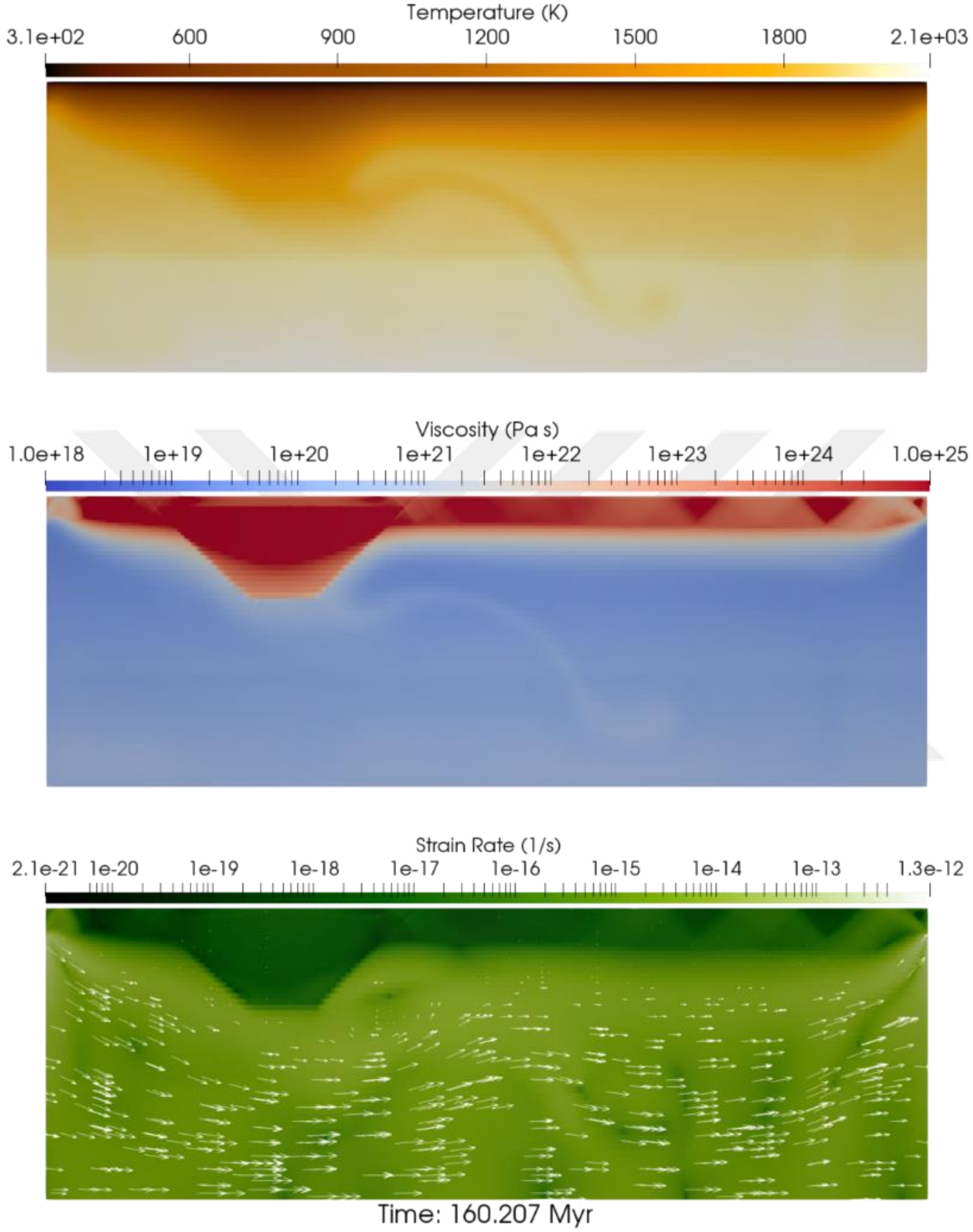

Figure 3.1 : Craton becomes mobilized at t = 160.207 Myr.

Moving craton continues to imbricate oceanic lithosphere as it moves and creates another eclogitic drip right on the periodic boundary. At t=186.449 Myr, moving craton subcretes oceanic lithosphere, resulting in formation of an eclogitic viscous drip on the right margin of the craton. (Figure 3.3).

Velocity vectors show that, both rift system on the left side and thickening of the oceanic crust on the right side contributes to the formation of this secondary drip. Sunken parts of denser oceanic lithosphere can be seen near the bottom right corner (Figure 3.4).

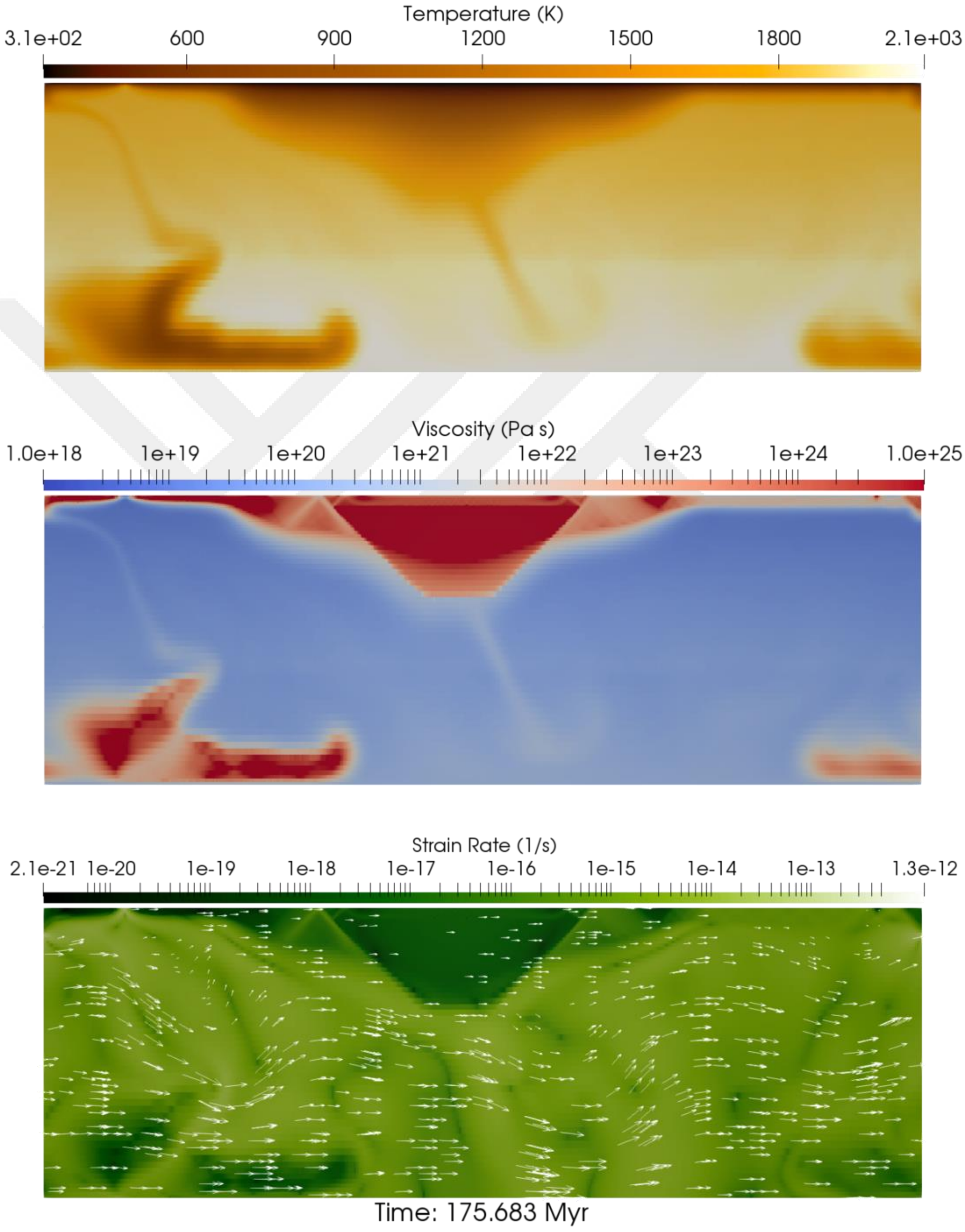

Figure 3.2 : A rift opens on the left side of the craton while some parts of oceanic lithosphere, located on the left and the right side of the craton, drifts away with the moving craton.

Drip formed by compression leads to even further lithospheric recycling. Which eventually leads to fertilized mantle rocks and lowered melting temperatures. Vector arrows show the direction of moving mantle and crustal rocks. There are two distinct convection cells are also observed near the model ending.

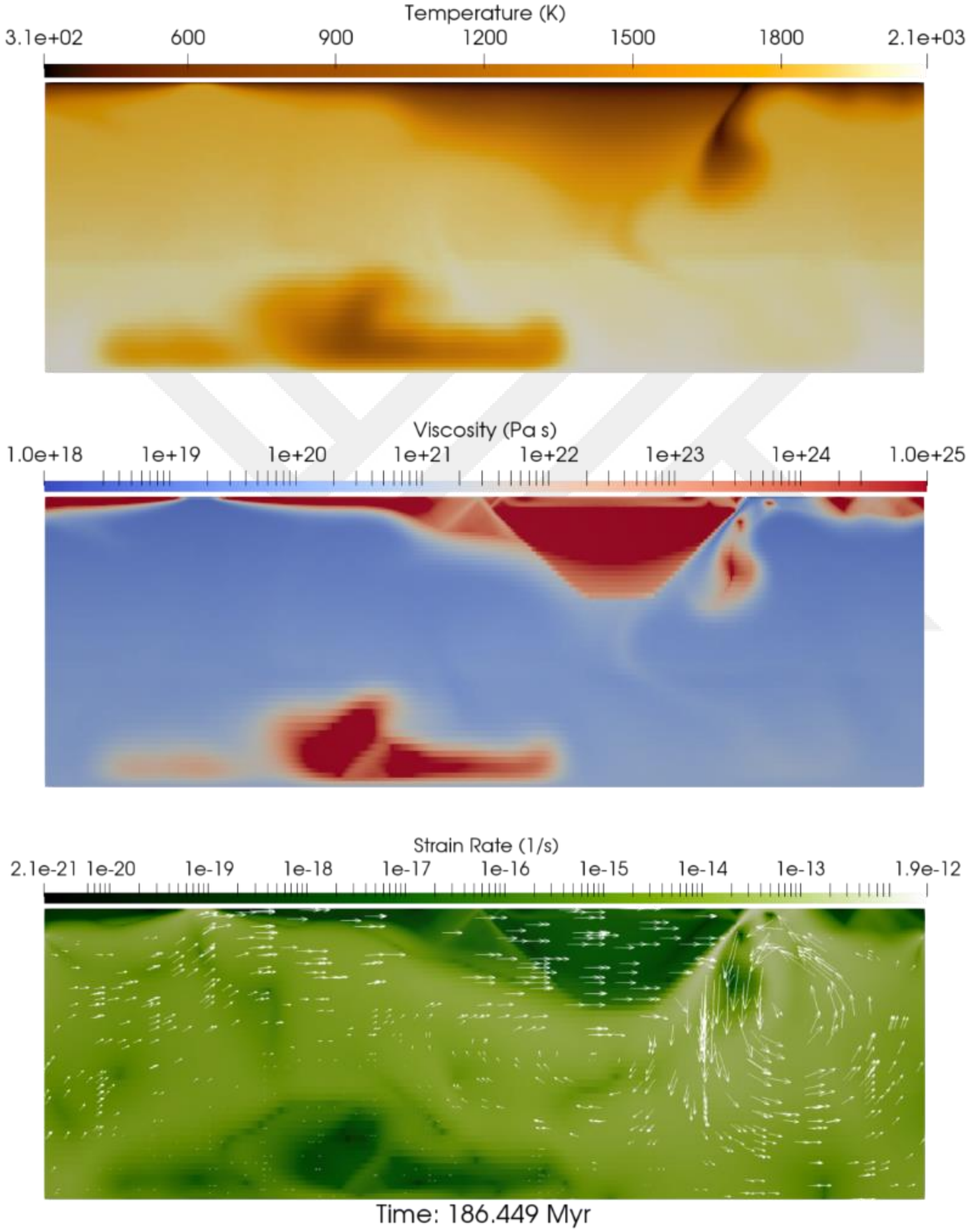

Figure 3.3 : Hot asthenospheric rocks rises through the opening near the left boundary, and oceanic lithosphere becomes subcreted at the right margin of the craton.

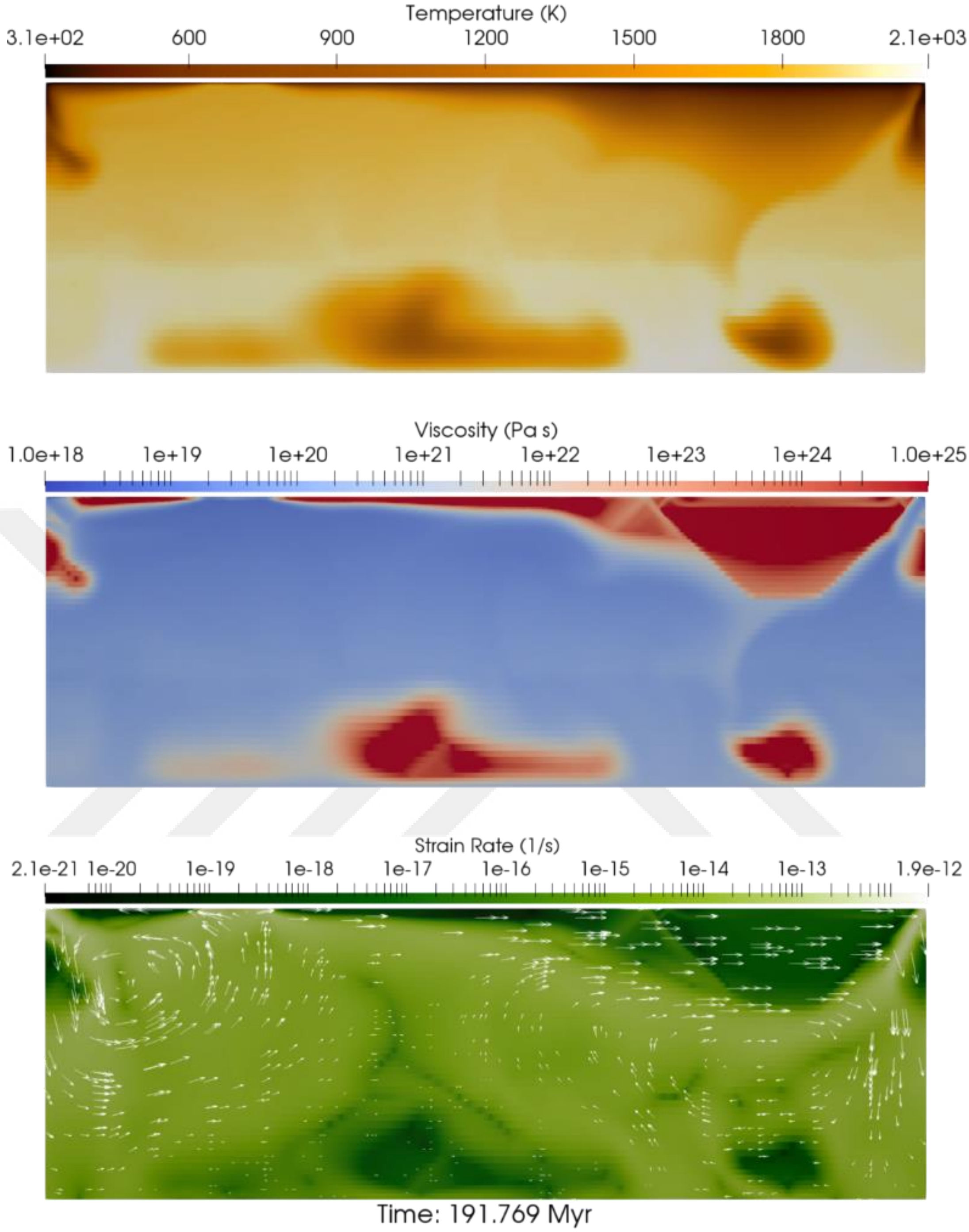

Figure 3.4 : Oceanic lithosphere gets compressed on the periodic boundary, gets thicker and eclogitizes.

3.2 Effects of Deformation Mechanism (Experiment A2)

In experiment A2, dislocation creep has been used to understand the effect of change in the deformation mechanism with respect to the reference model A1. To provide a suitable comparison between the two models all parameters are kept same with the reference model except for the deformation mechanism. This means that, surface yield stress has chosen to be 20 MPa. All other model parameters used in numerical calculations are given in (Table 3.2).

Table 3.2 : Model Parameter for Experiment A2

Experiment # A2		
Reference Mantle Viscosity	10^{20}	Pa s
Surface Yield Stress	20	MPa
Friction Coefficient	0.1	
Thermal Anomaly Size	0.5	
Eclogite Phase Transition Depth	40	km
Cohesion	10^{3}	Pa
Deformation Mechanism	Dislocation	
Continent Radius (km)	300	km
Mantle Flow Velocity	4	cm/yr
Mantle Flow Starting Depth	60	km

Craton starts to drift away approximately around 190 Myr. Movement of the craton creates a counter-clockwise convective motion in the mantle, on the right side of the keel. Near the right boundary, oceanic lithosphere thickens while a rift starts to open next to the left boundary. Vector arrows shows an undulation near the bottom boundary. (Figure 3.5).

Phase transition from basaltic oceanic crust to eclogite near the right boundary takes place around ~200 Myr. Eclogitized oceanic crust becomes denser and develops a gravitational instability in the form of a viscous drip. Rift forming on the left side enlarges while a small part of oceanic lithosphere drifts away with the craton. Small scaled overturn created by the eclogitic drip leads asthenosphere through the surface, possibly leading to formation of new basaltic crust due to decompression melting (Figure 3.6).

When t = 205.981 Myr, oceanic basaltic lithosphere moving attached to the craton, starts to get thicker by subcretion under the influence of sub-lithospheric mantle flow. Eclogitized basaltic crust forms another drip on the left margin of the craton. Meanwhile, asthenospheric rocks cools down to form new generation of oceanic crust on the right side of the box (Figure 3.7).

Subcreting oceanic lithosphere on the right side, eventually gets sufficiently thick enough to form another eclogitic drip. Vector arrows reflect an increase in the acceleration on the dripping zone (Figure 3.8).

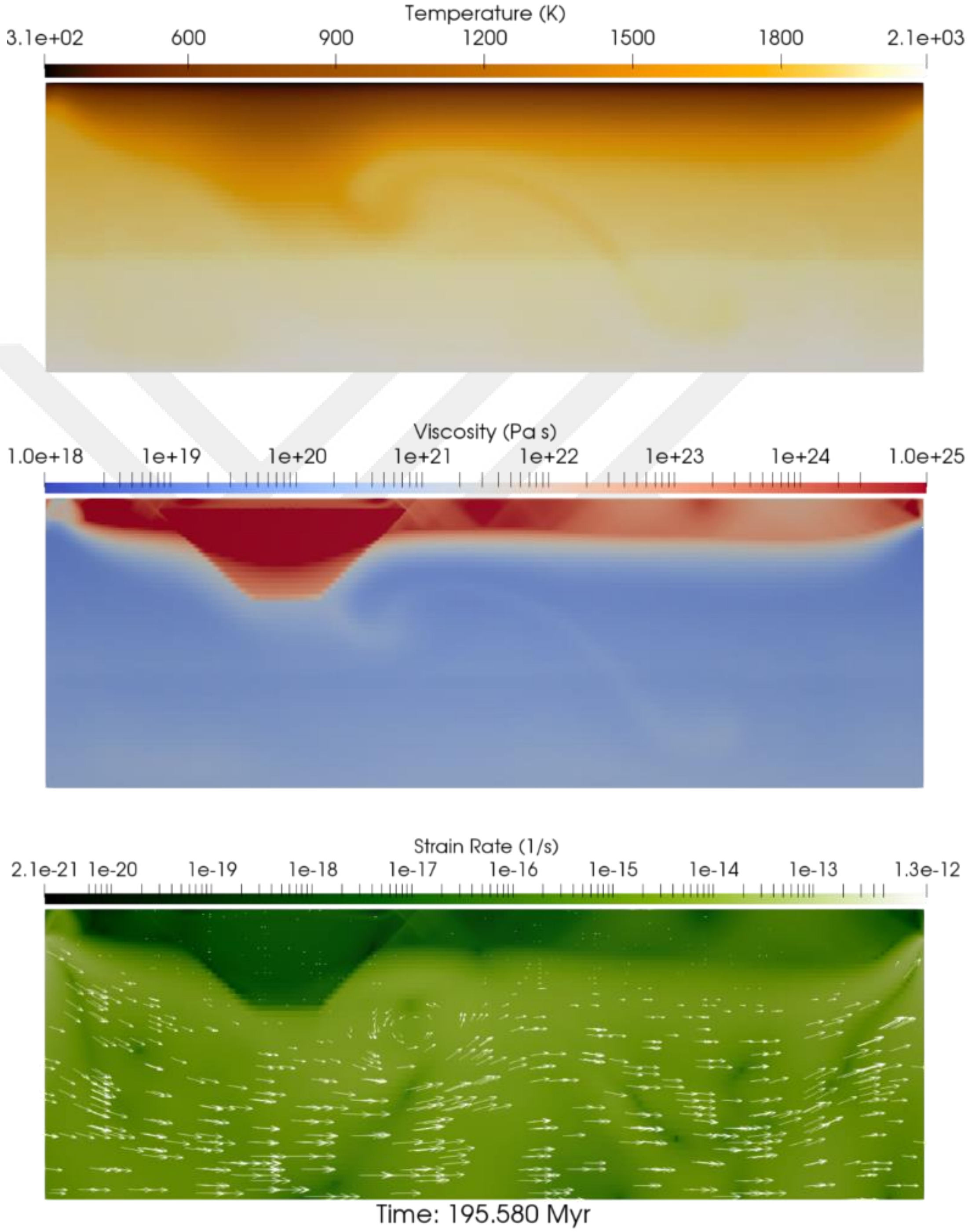

Figure 3.5 : Dislocation creep extends mobilization time around ~35 Myr.

Change from diffusion creep to dislocation creep, creates a stiffer oceanic lithosphere. As a result, deformation of the oceanic lithosphere is clearer, especially at the cratonic margins. Stresses needed to deform the craton is much higher, and as a result, oceanic part attached to the left side of the craton due to mantle winds, subcretes at the margin.

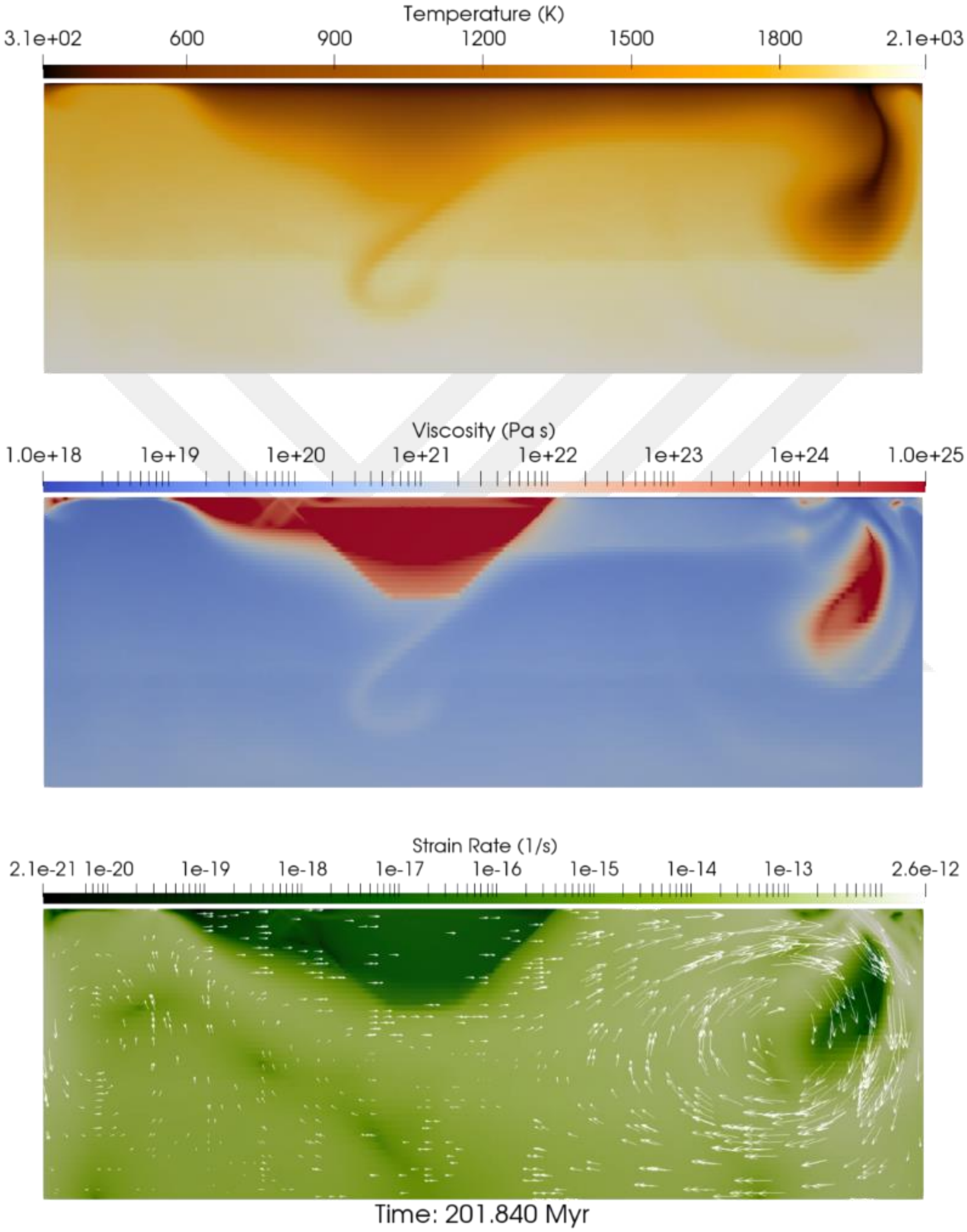

Figure 3.6 : Phase transition of the oceanic parts into eclogite creates an eclogitic drip on the right, and a rift opens on the left side where the oceanic crust became weaker and thinner

Results indicate that, subcretion does not always necessarily has to be on the right side which the cratonic keel is drifting, when the proper conditions are met under the influence of a counter-clockwise directed convective movement.

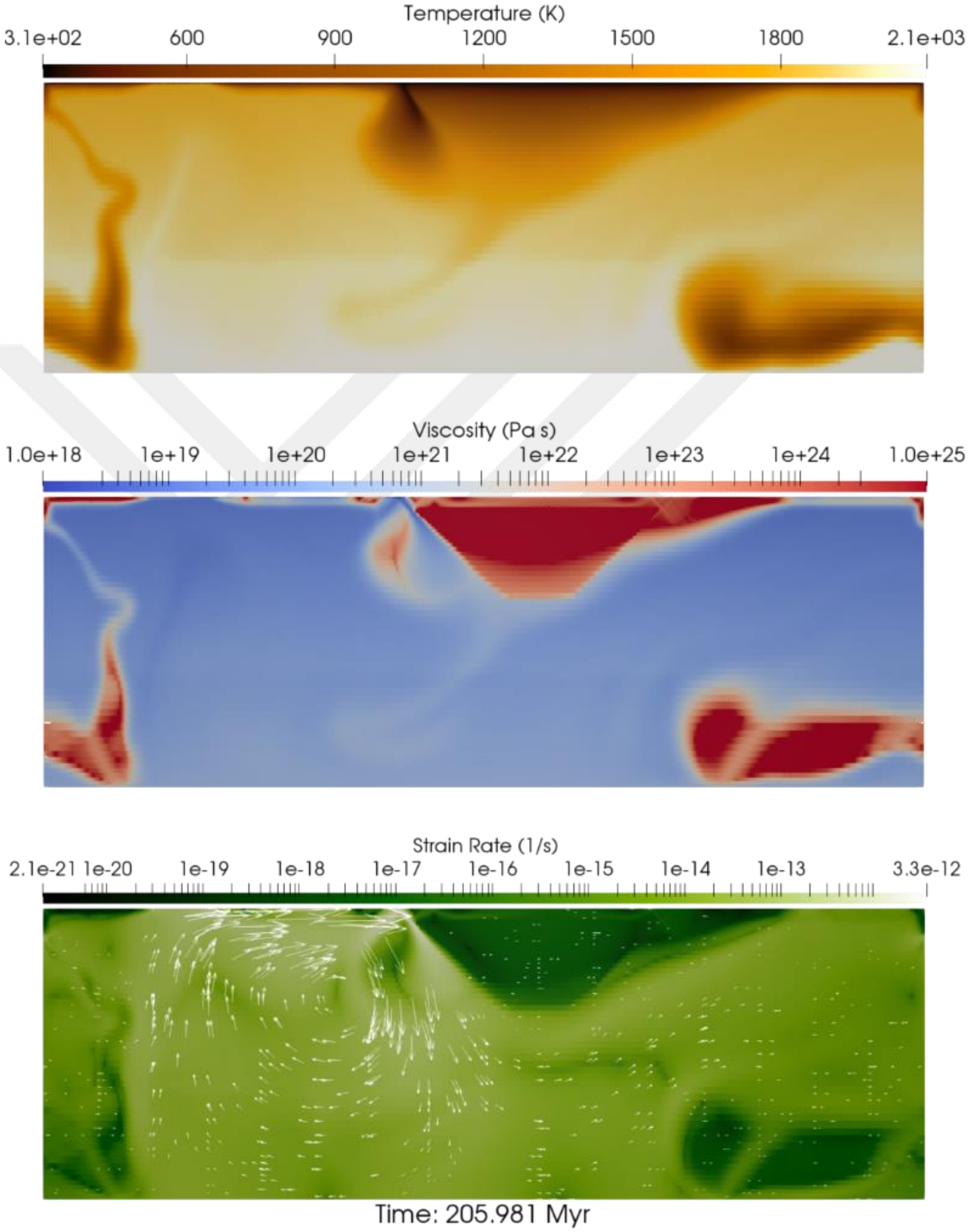

Figure 3.7 : Oceanic lithosphere attached to the craton, subcretes and eclogitizes at the left margin. Another rift starts to open on the right side of the craton. Craton stalls (and even moves a bit backwards) due to direction of convecting cells.

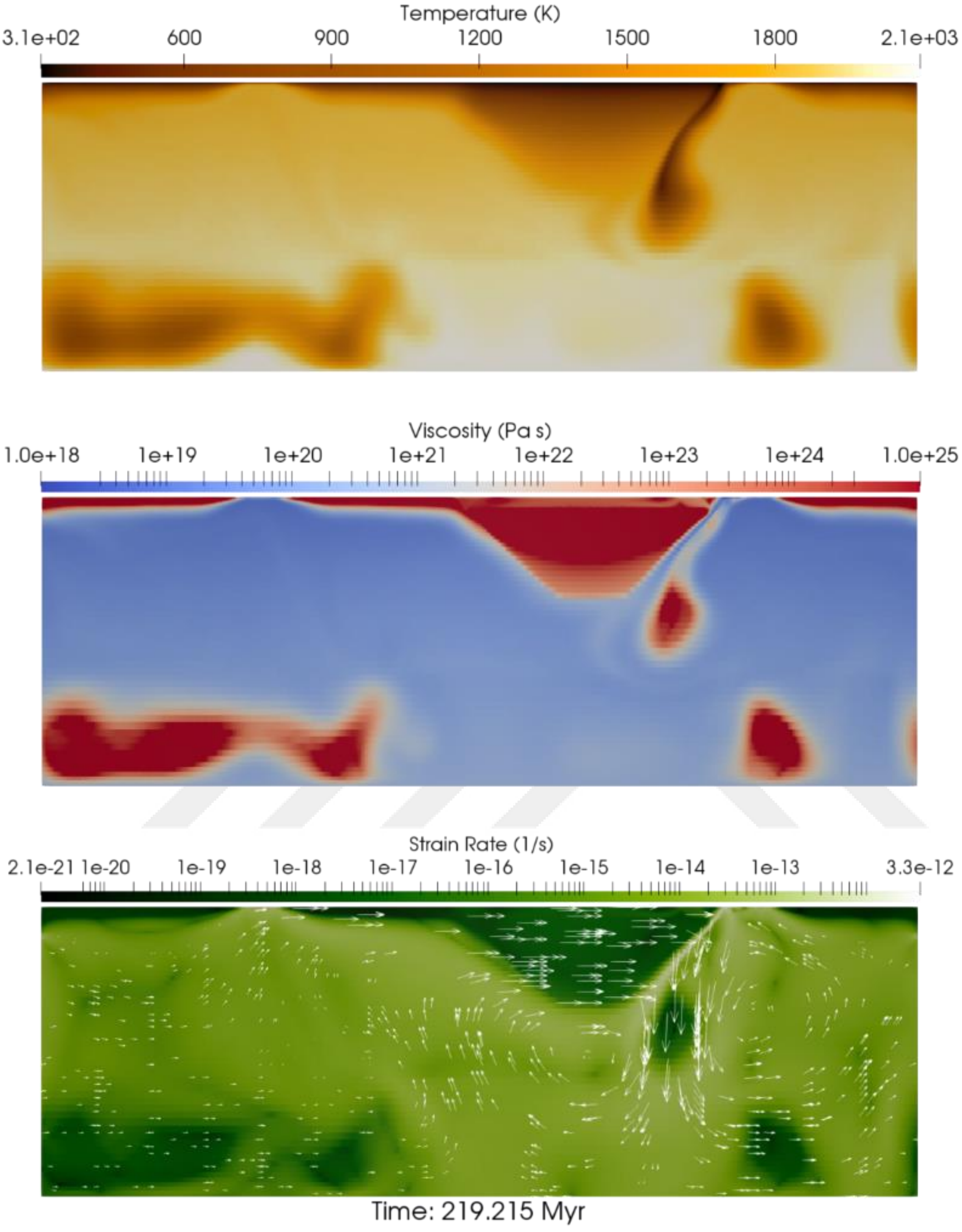

Figure 3.8 : Asthenospheric rocks rising from the rift located on the right, helps to the subcretion of oceanic lithosphere.

3.3 Effects of Surface Yield Stress (Experiments B1, B2 & B3)

In this experiment set, three different models; Experiment B1, Experiment B2 and Experiment B3 had been conducted to investigate the effect of yield stresses with respect to reference model. Yield stress can easily change the evolution of the model, because it defines the strength of the oceanic lithosphere. Higher yield stresses results in stronger oceanic lithosphere while its decline can make crustal and lithospheric rocks easily deformable.

3.3.1 Experiment B1

Parameters used for the Experiment B1 are given in Table 3.3 for comparison. Surface yield stress has chosen to be slightly higher than the reference model. As a result, strength of the craton is a bit higher than the reference model. Craton starts to drift away at t=207.426. Faulting occurs near the ocean-continent border and offshore oceanic lithosphere parts near the right boundary (Figure 3.9).

5 MPa difference in the yields stress delays the mobilization of the craton 47 Myr. After 20 Myr, craton migrated around 500 km from its starting position, a ridge have formed on the left side of the craton, and thickened oceanic lithosphere have sunk in the asthenosphere in the form of viscous Rayleigh-Taylor drips. Erosive nature of the hot mantle rocks, creates insignificant deformation at the base of the strong durable cratonic root (Figure 3.10).

Strengthen oceanic lithosphere does not subcrete on the edge of the craton like it does on the reference model. It drifts away with the craton until it thickens due to craton push and counterclockwise motion of the convection cell located on left-hand side on Figure 3.11.

Table 3.3 : Model parameters for Experiment B1.

Experiment # B1		
Reference Mantle Viscosity	10^{20}	Pa s
Surface Yield Stress	25	MPa
Friction Coefficient	0.1	
Thermal Anomaly Size	0.5	
Eclogite Phase Transition Depth	40	km
Cohesion	10^{3}	Pa
Deformation Mechanism	Diffusion	
Continent Radius (km)	300	km
Mantle Flow Velocity	4	cm/yr
Mantle Flow Starting Depth	60	km

Sunken parts of the oceanic lithosphere can also transport crustal material, volatiles and incompatible elements into the mantle. Temperature field shows that rising hot mantle rocks contributes to the cooling of the inner Earth. Which can decrease the mantle temperatures in time and decrease viscosity of the mantle rocks.

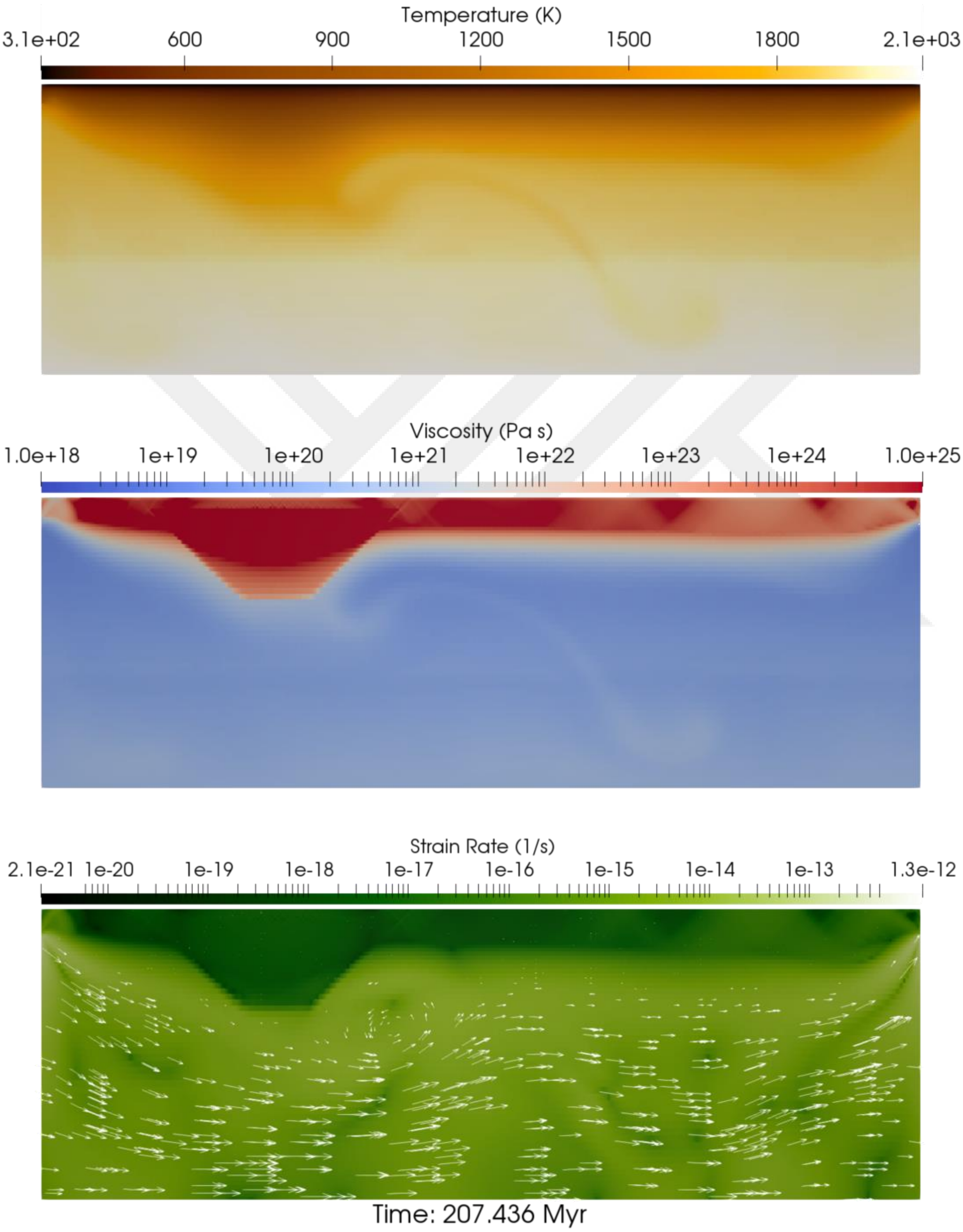

Figure 3.9 : The craton starts to drift away at t = 207.436 Myr.

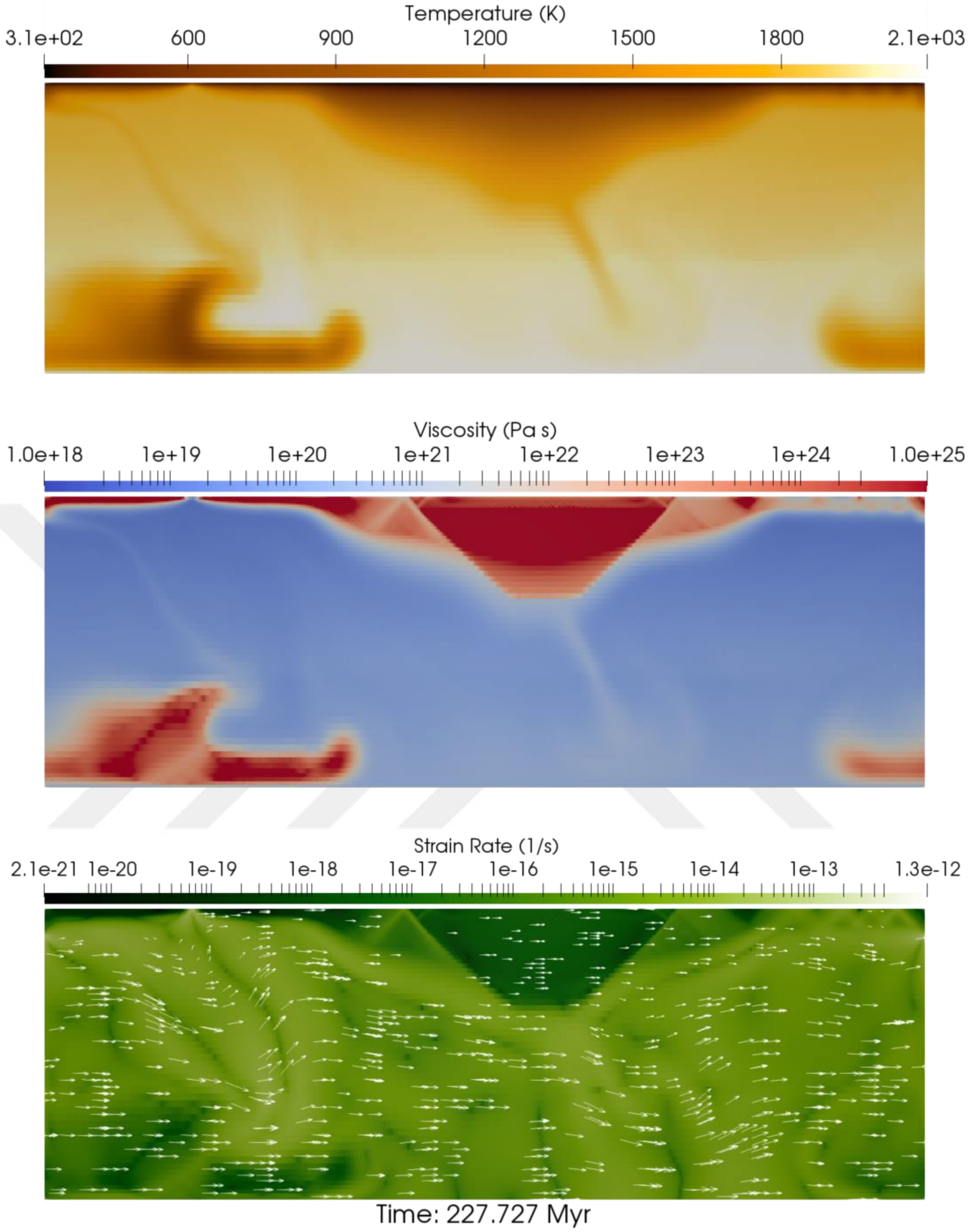

Figure 3.10 : Thickened parts of oceanic lithosphere drips away, and a ridge forms on the left side of the craton

Although viscosity is temperature dependent in numerical calculations, temperature change due to cooling was not implemented in models. Thus, one model is not enough to make assertive claims. Nonetheless, separate models combined can draw a clear picture for further implications and deductions.

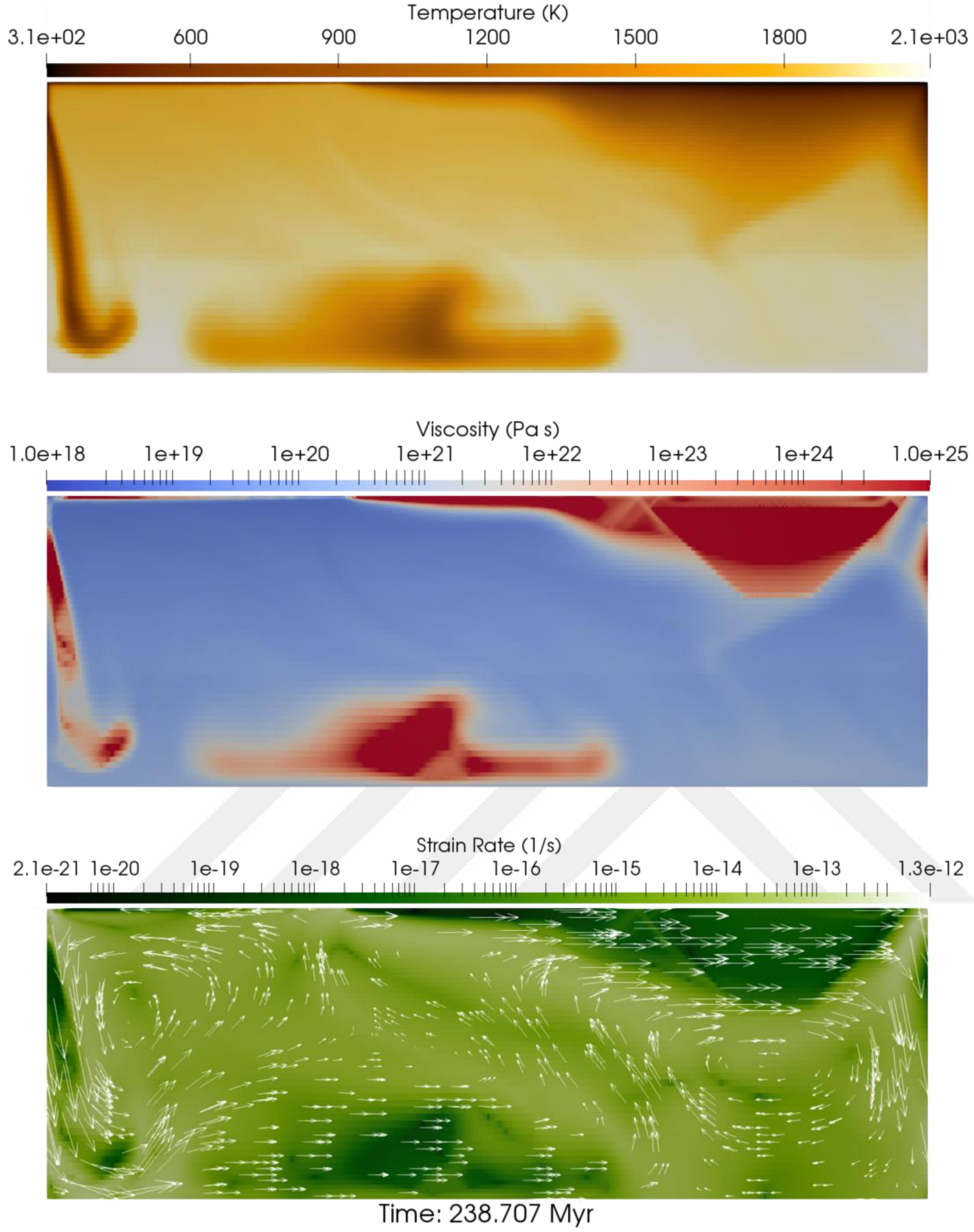

Figure 3.11 : A drip along the periodic boundary forms due to craton push and counterclockwise convection cell.

3.3.2 Experiment B2

For Experiment B2, surface yield stress has chosen to be 30 MPa, and deformation depends on diffusion creep. Reference mantle viscosity, is the same as the previous model. Friction coefficient, eclogite phase transition depth and cohesion values are given in Table 3.4.

Increased surface yield stress results in rheologically stronger oceanic lithosphere compared with the reference model. As a result, mobilization of the craton does not occur until 318 Myr. Faulting near the ocean-continent boundary forms due to compression caused by movement of the craton. Undulation of the vector arrows near the bottom boundary are most likely due to small thermally eroded parts from cratonic keel and/or oceanic lithosphere Sudden decrease in the viscosity of some of the oceanic lithosphere parts are represented with a light red in the viscosity gradient color scheme (Figure 3.12).

Table 3.4 : Model Parameters for Experiment B2

Experiment # B2		
Reference Mantle Viscosity	10^{20}	Pa s
Surface Yield Stress	30	MPa
Friction Coefficient	0.1	
Thermal Anomaly Size	0.5	
Eclogite Phase Transition Depth	40	km
Cohesion	10^{3}	Pa
Deformation Mechanism	Diffusion	
Continent Radius (km)	300	km
Mantle Flow Velocity	4	cm/yr
Mantle Flow Starting Depth	60	km

At t=323.19 Myr, two distinct convection cells are observed near the left and the right boundaries, one is counter-clockwise while the other one is clockwise, respectively. Flows generated within the asthenosphere due to these convection cells, thickened the crust and led to formation of an eclogitic drip. Meanwhile, two rift systems are formed because of the direction of motion of the convection cells, next to left and right margins of the craton (Figure 3.13).

Results obtained from Experiment B2 show that, even 10 MPa difference in surface yield stresses can create a significant difference relative to the reference model. Throughout the evolution of the model, oceanic lithosphere is deformed by the eclogitization when the needed P-T conditions are met, but any type of orogenic activity have not been observed as seen on the several other models mentioned previously.

Drastic changes resulted from small difference in the parameter space prove that there is a sharp boundary in the between subcretion and drip dominated geodynamic regime aside from the elongated mobilization times. Around 320 Myr vector arrows in the model show that fast flow is limited to the lower mantle until the craton starts to move. Upper stagnant part also effects velocities on the bottom of the lithosphere. Mantle flows coming in contact with these parts slow down and perturbations beneath the ocean-continent border creates small-scaled thermal convection cells, which might be a leading factor in pulling oceanic lithosphere down, even though that is not the case in this particular experiment.

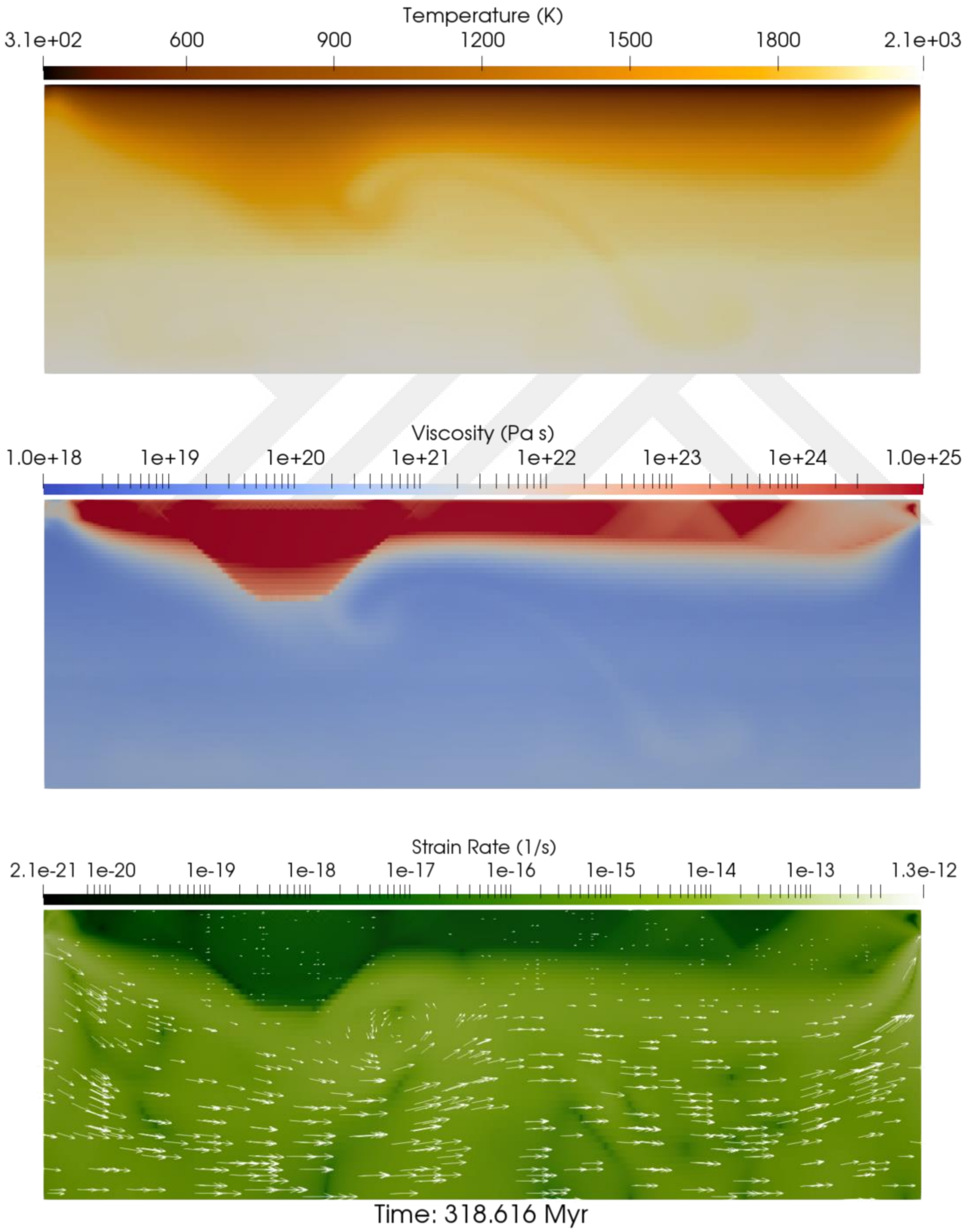

Figure 3.12 : Craton becomes mobilized ~150 Myr later from previous models.

Sunken oceanic parts disturb the mantle flows as they are going down. This may create an upwelling in the mantle rocks, which can lead to higher heat flux through a particular region. Increased heat flux may lead to high degrees of melting which in turn, create more dense mafic rocks along these regions.

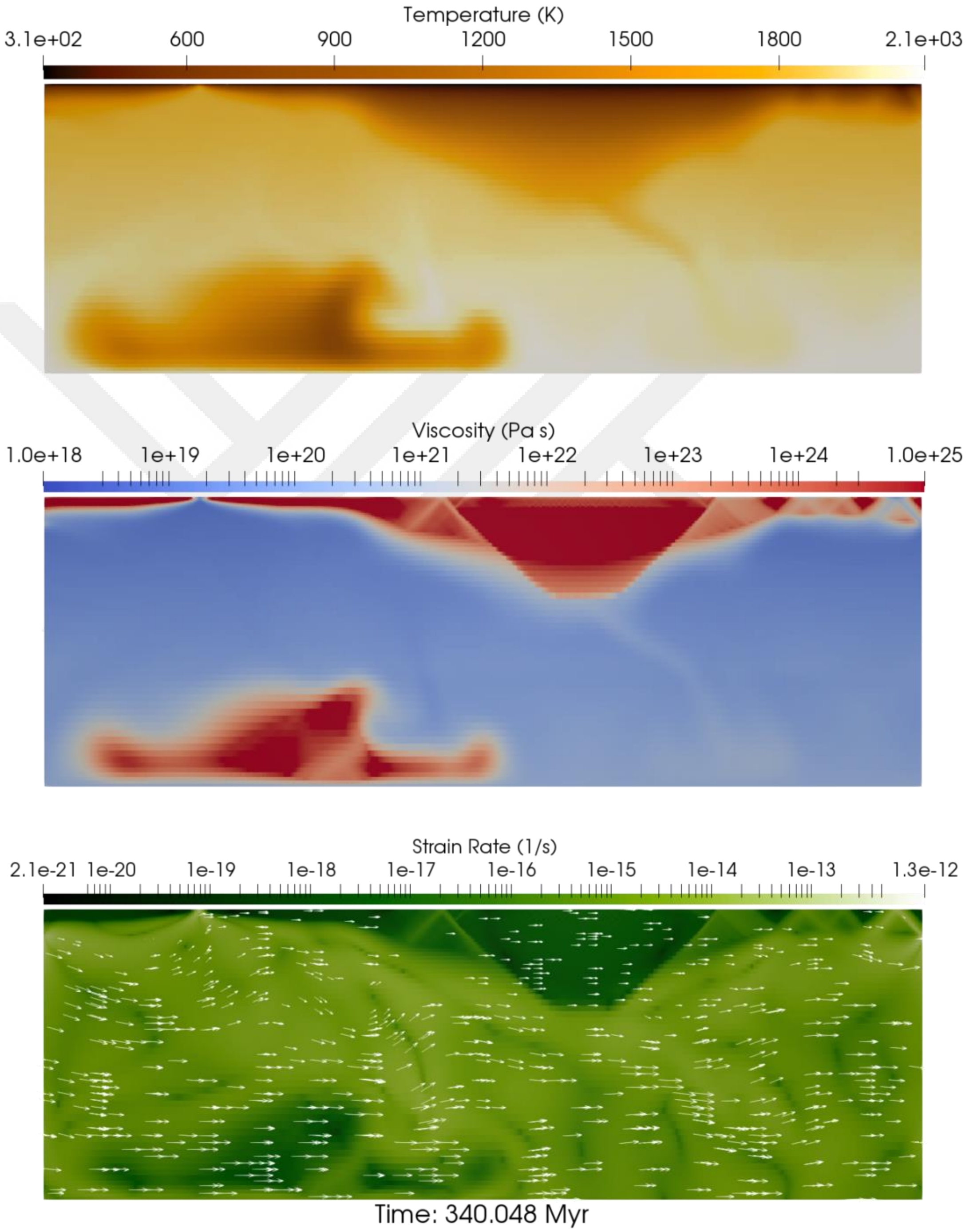

Figure 3.13 : Rifting on the left side results in generation of new oceanic crust. Meanwhile, oceanic lithosphere becomes thicker near the right boundary.

3.3.3 Experiment B3

Experiment B3 is conducted even with higher yield stresses to fill up the parameter space. Other related parameters are given in Table 3.5. Expectedly, stronger oceanic lithosphere had not yielded this time and craton stayed stable until the last time step (476 Myr).

Table 3.5 : Model Parameters for Experiment B3

Experiment # B3		
Reference Mantle Viscosity	10^{20}	Pa s
Surface Yield Stress	40	MPa
Friction Coefficient	0.1	
Thermal Anomaly Size	0.5	
Eclogite Phase Transition Depth	40	km
Cohesion	10^{3}	Pa
Deformation Mechanism	Diffusion	
Continent Radius (km)	300	km
Mantle Flow Velocity	4	cm/yr
Mantle Flow Starting Depth	60	km

Through the end of the model, a rift, an important candidate to trigger deformation, on the periodic boundary appears to be forming (Figure 3.14). If even that is the case, 10 MPa difference in the surface yield stress can result in ~100 Myr stalling in the mobilization of craton. Arguably, reference mantle viscosity might not be sufficiently high to apply the needed pressure onto the cratonic keels. Therefore, orogeny related deformation of rheologically stronger oceanic lithosphere requires further investigation under various mantle viscosity values.

Experiment B3 implies that, between the 30 MPa and 40 MPa, there is a sharp boundary. On the higher side of this boundary oceanic lithosphere becomes almost undeformable for ~500 Myr (i.e. valid for the given parametric conditions). This also indicates that transition from stagnant-lid to plate tectonics (or episodic subduction) might be due to these small changes in the yield stresses.

Yield stresses of rocks can become lower due to increasing temperatures. Temperature increase might be due to hot upwellings caused by previous downwellings and/or mantle plumes. Heated rocks allow for a easily deformable environment which can create subductions on the Earth.

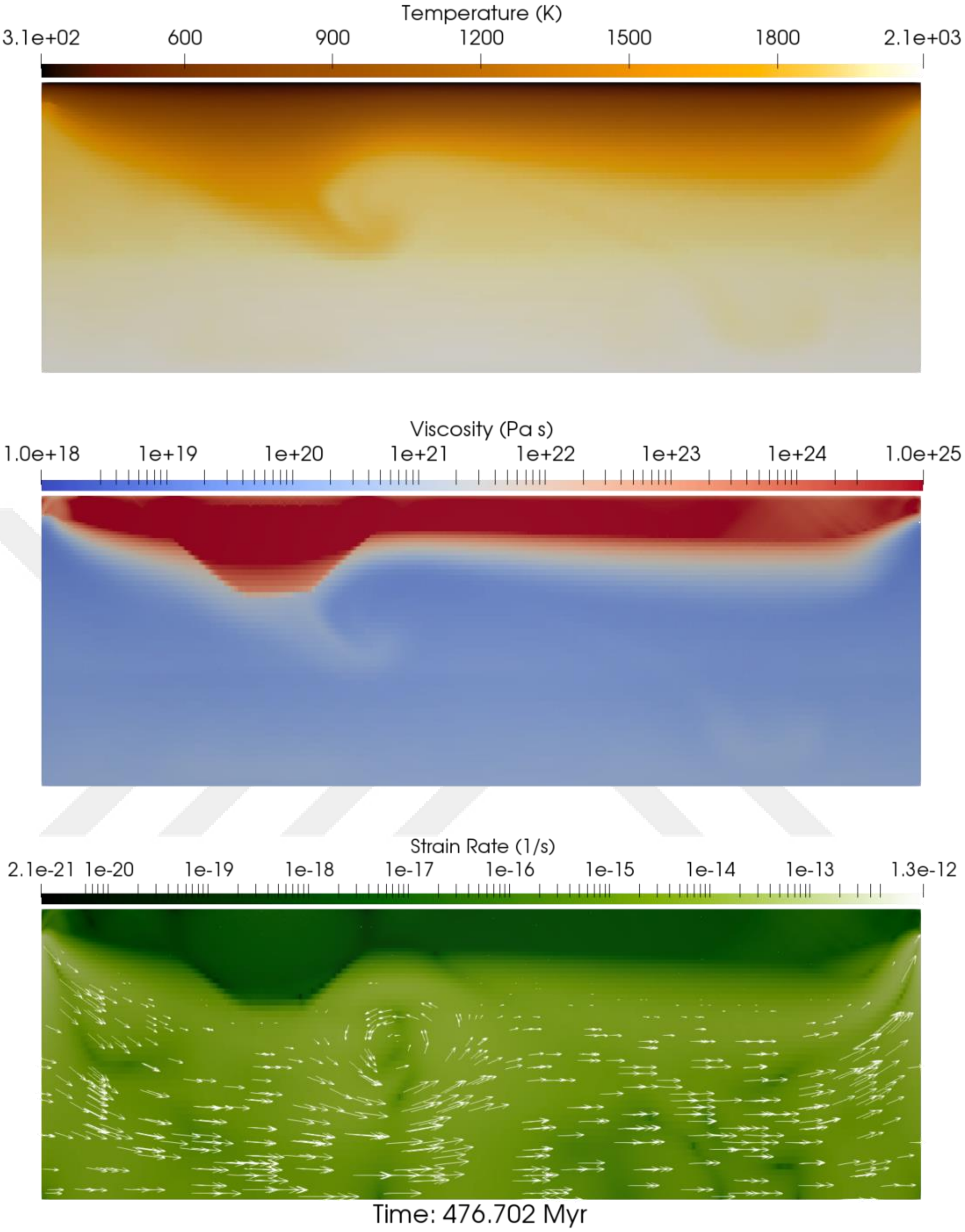

Figure 3.14 : When surface yield stress is 40 MPa, craton does not drift away under given conditions.

3.4 Effects of Eclogite Transition Depth (Experiment C1 & Experiment C2)

Eclogite phase transition depth controls the eclogitization depth of basalts within the model. Eclogite facies can be stable on a widely ranging scale of temperature and pressure, usually when temperatures are above 500 ºC and pressures are more than

1.2 GPa (Hacker, 1996). Consequently, impact of variations in the phase transition depths of eclogite are observed in this experiment set, varying from 40 km, the depth used in the reference model, to 50 km and 60 km in Experiment C1 and C2, respectively.

3.4.1 Experiment C1

In Experiment C1, eclogite phase transition starts at a depth of 50 km. All of the other parameters are same as the reference model to clearly see the effect of eclogite phase transition depth (Table 3.6). In this case, craton starts to move after ~136 Myr. Drifting craton starts to apply stress on the oceanic lithosphere. This creates stacking and faulting along the relatively weaker parts on the oceanic lithosphere. At the ocean-continent border there is a fault moving through the continental crust. The faults are reaching through the mantle along oceanic lithosphere due to relatively brittle nature of the basaltic crust (Figure 3.15).

Table 3.6 : Model Parameters for Experiment C1.

Experiment # C1		
Reference Mantle Viscosity	10^{20}	Pa s
Surface Yield Stress	20	MPa
Friction Coefficient	0.1	
Thermal Anomaly Size	0.5	
Eclogite Phase Transition Depth	50	km
Cohesion	10^{3}	Pa
Deformation Mechanism	Diffusion	
Continent Radius (km)	300	km
Mantle Flow Velocity	4	cm/yr
Mantle Flow Starting Depth	60	km

Around 4-5 Myr later, oceanic lithosphere gets thicker at edges and it starts to sink into the asthenosphere. Clockwise moving convection cell near the right boundary, steers mantle wind upwards as can be seen by the velocity vectors. A part of oceanic lithosphere becomes attached on the left side of the craton due stresses applied by the upwelling mantle rocks, while another part is pushed away by the craton as it moves. Because of this there are two distinct faults formed around the craton. Upwelling mantle on the left and right sides near the boundaries force oceanic lithosphere downwards (Figure 3.16).

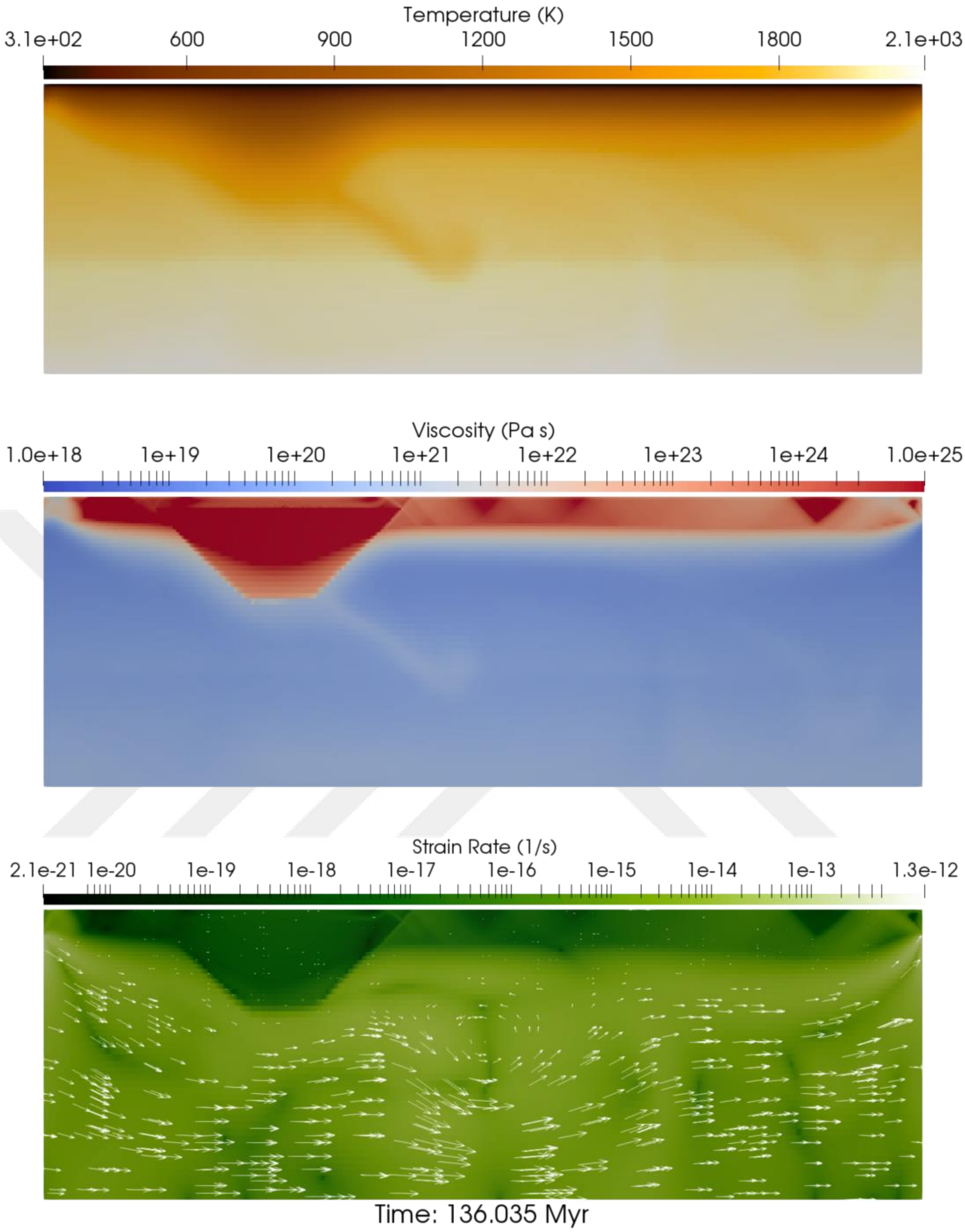

Figure 3.15 : Craton starts to drift away at t=136.035 Myr.

Deflected asthenospheric mantle winds drive the craton backwards until the point that the convection cell deflecting the mantle winds fades away. After that point, craton continues its rightward movement and subcretes oceanic lithosphere at its margin as seen on the reference model. It pulls down a thin layer of oceanic lithosphere with it while sinking. Meanwhile, accretion along the oceanic parts near the right boundary occurs. Mantle flow velocities drastically drops near the lower mantle because of the interruption caused by downwelling parts of oceanic lithosphere. On the other hand, upper parts near lithosphere-asthenosphere boundary, do not seem to be affected much by the disturbance caused by removed lithospheric parts (Figure 3.17).

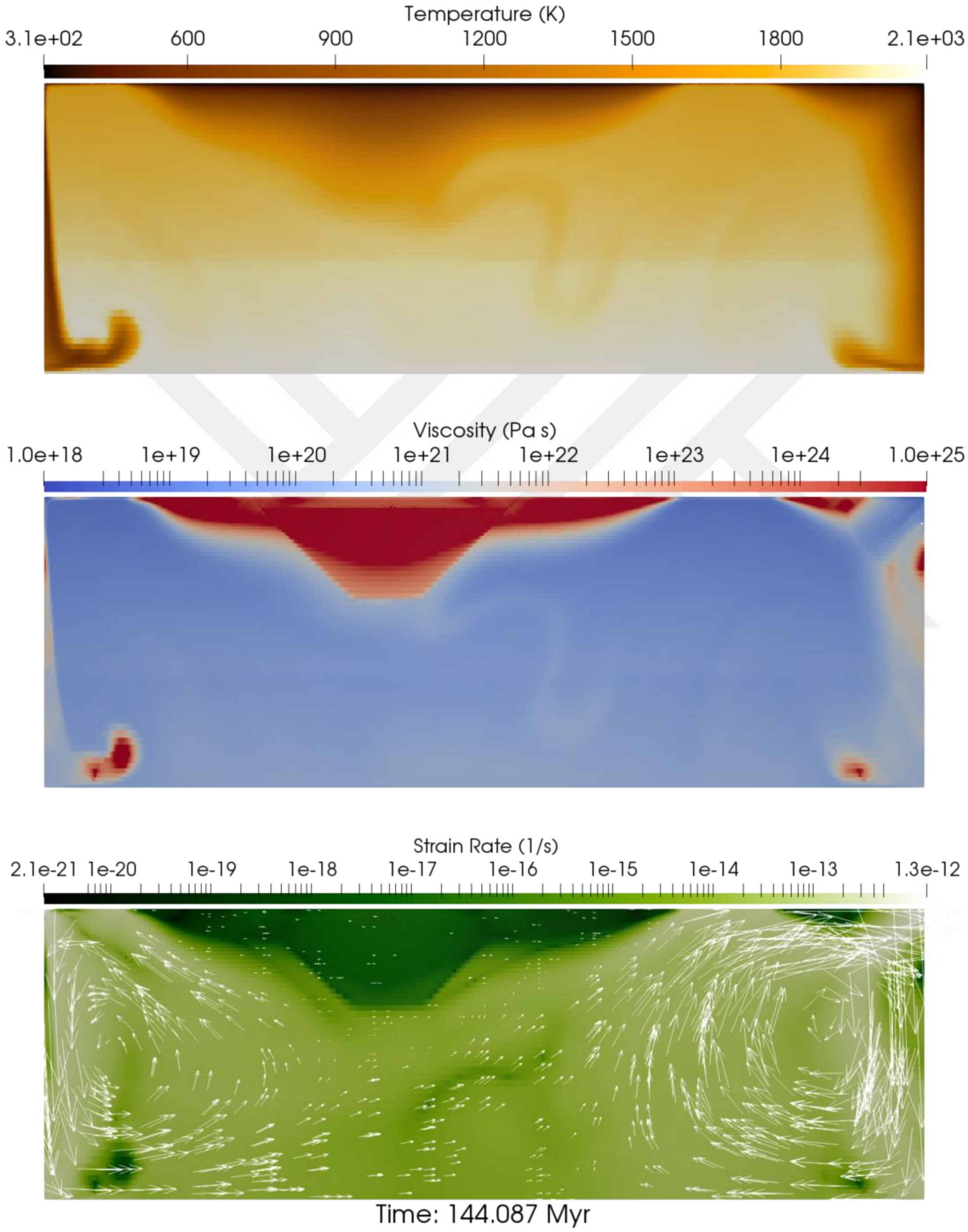

Figure 3.16 : Eclogitic drip forming on the periodic boundary due to crustal thickening.

Subcretion of oceanic lithosphere fertilize the mantle rocks with incompatible elements and water. As the model suggests it is not the only viable mechanism for crustal recycling, but it can be a viable mechanism for the formation of TTG suites.

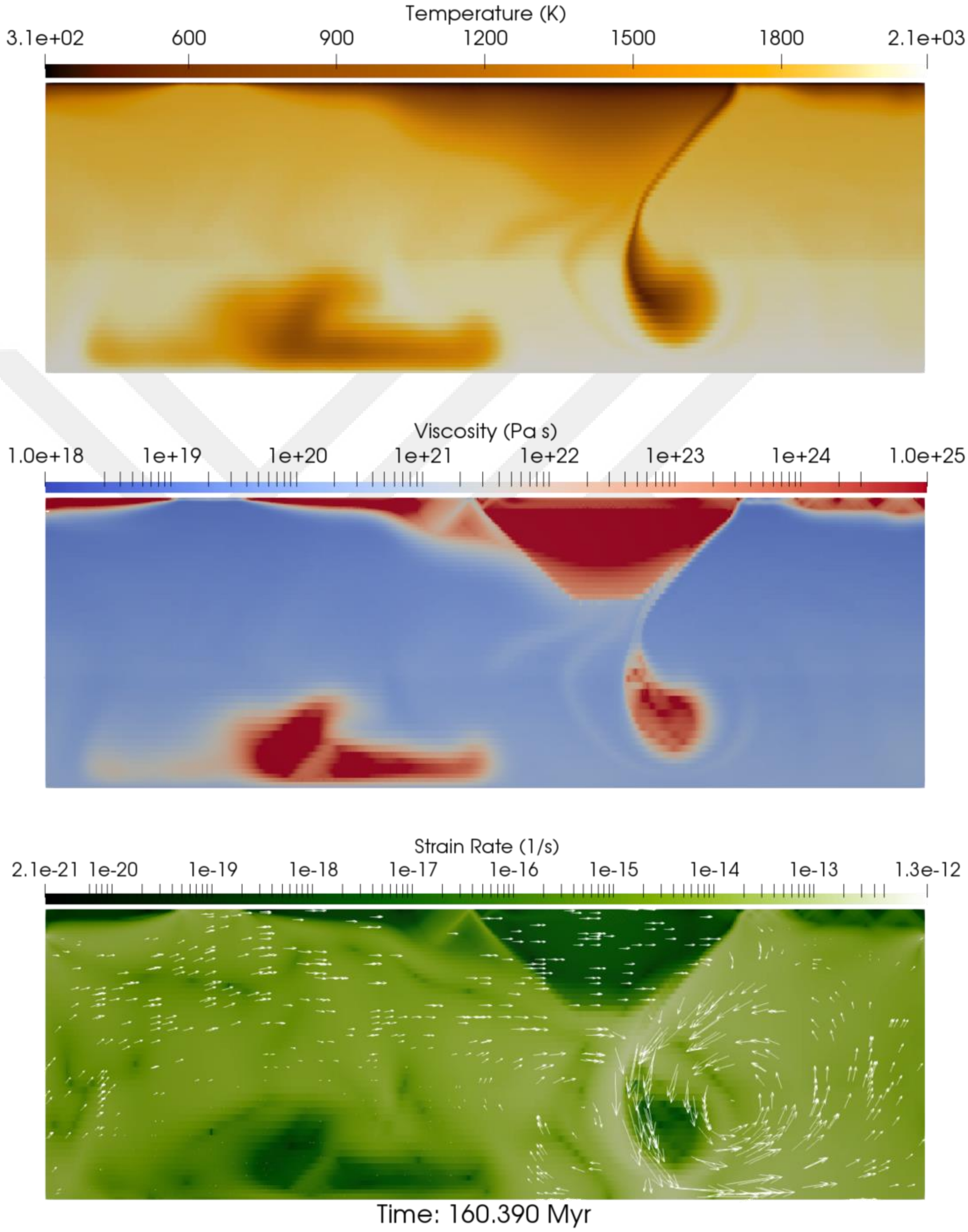

Figure 3.17 : Subcreted basaltic oceanic crust becomes denser due to eclogitization and sinks as a viscous drip.

3.4.2 Experiment C2

Only difference between the reference Experiment C2 and Experiment C1 is that eclogite phase transition starts at a 60 km depth. Other parameters used in numerical calculations such as reference mantle viscosity, surface yield stress and friction coefficient are given in Table 3.7.

Table 3.7 : Model Parameters for Experiment C2.

Experiment # C2		
Reference Mantle Viscosity	10^{20}	Pa s
Surface Yield Stress	20	MPa
Friction Coefficient	0.1	
Thermal Anomaly Size	0.5	
Eclogite Phase Transition Depth	60	km
Cohesion	10^3	Pa
Deformation Mechanism	Diffusion	
Continent Radius (km)	300	km
Mantle Flow Velocity	4	cm/yr
Mantle Flow Starting Depth	60	km

Craton starts to drift away around 150 Myr and rising asthenosphere from the left leads to crustal thickening and eclogitization of basaltic crust. Viscosity of big chunks of oceanic lithosphere decrease due to heat coming from rising asthenospheric rocks located on the right side of the craton (Figure 3.18).

At t = 178.531 Myr, oceanic lithosphere near the right boundary gets thicker due to compressional forces applied by the drifting craton. A narrow rift opens up on the left-hand side of the moving craton. While a stacked terrane starts to form on the right-hand side of the craton due to compressional forces caused by the cratonic mobilism. Because of the higher eclogitization depth oceanic lithosphere stays more intact compared with the previous model (Experiment C1). Stacking of the oceanic lithosphere resemble to early stages of continent-continent collision (e.g. India-Eurasia collision). Yet the absence of another continental fragment did not allow for a similar evolution (Figure 3.19). It can be argued that with the implementation of another continental part, a fully developed stacked terrane would develop resembling to modern day Himalayan orogenic belt. However, continental collision and topography caused by it is beyond the scope of this study.

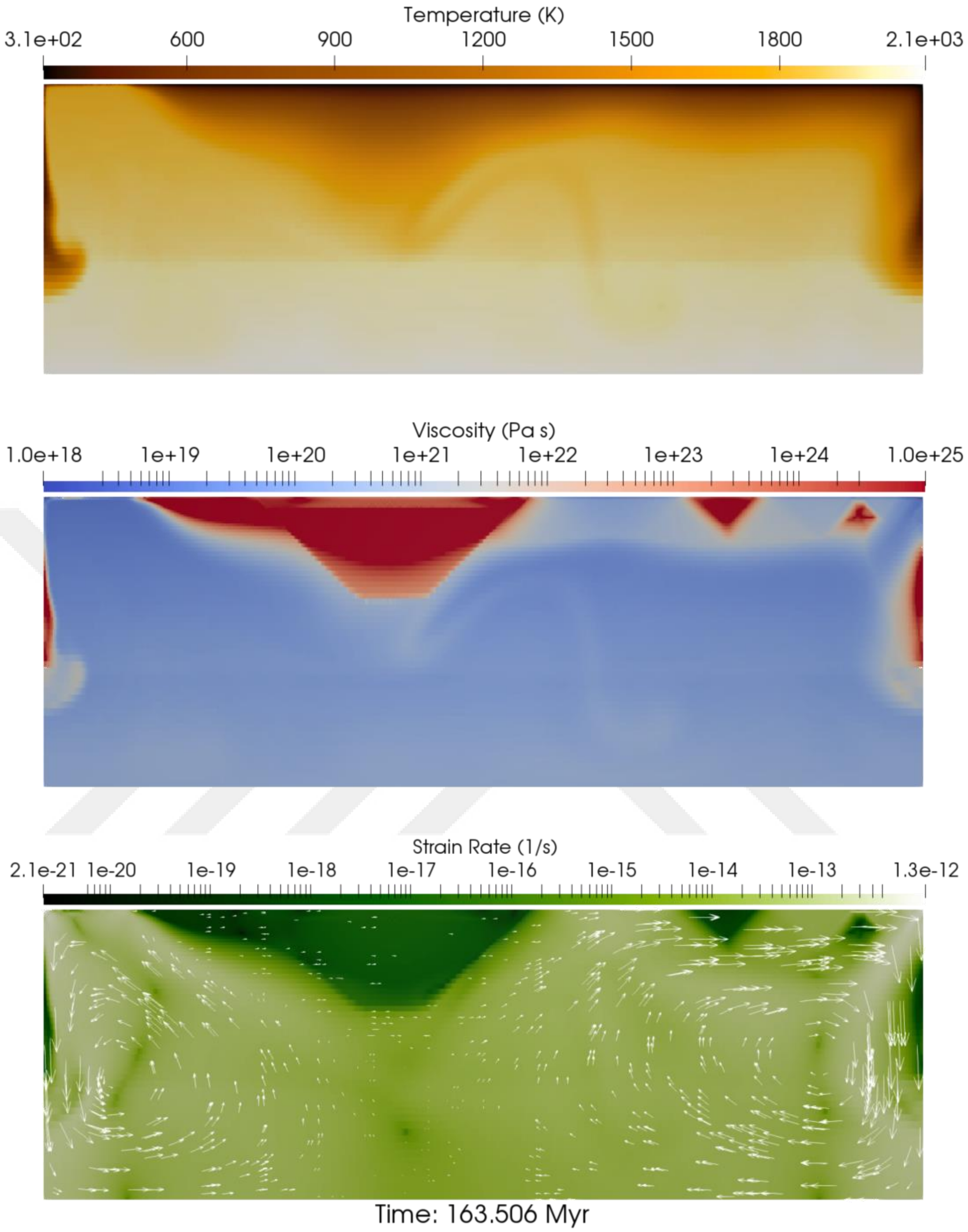

Figure 3.18 : Asthenosphere rises through the rift formed on the left-hand side. Basaltic crustal material undergoes phase transition into eclogite and forms and eclogitic drip.

Displacement of craton results in disruption of the terrane formed near the right boundary. Further compression caused by the craton results in a secondary drip on the periodic boundary. This downgoing movement of a part of oceanic lithosphere creates a counter-clockwise moving convection near the left boundary. While it is the opposite on the right side of the figure (Figure 3.20).

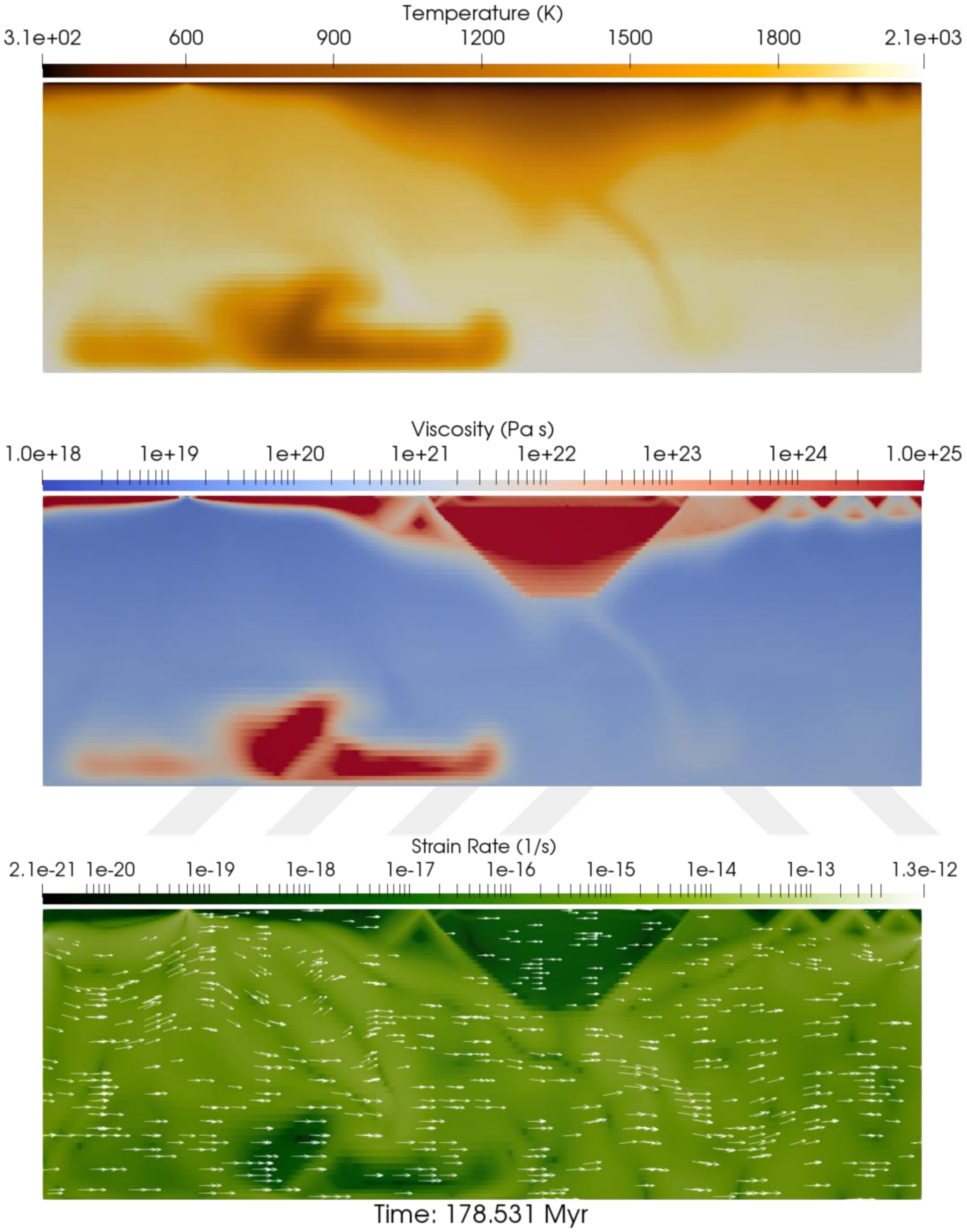

Figure 3.19 : Oceanic lithosphere gets thicker on the right side due to compressional forces.

Arguably, periodic boundary conditions might provide a more suitable environment for the formation of eclogitic viscous drips along the oceanic lithosphere, because upwellings combined with the drifting craton creates stresses from both sides at the same time. However, in our case periodic boundary conditions are more suitable because of the constant flow starting after the first 60 km depth. This way; physical, chemical and compositional properties of the material is always the same. Also, by using periodic conditions, any defect that can be caused by the small calculation errors in the mass balance can be eliminated. If a closed box with free slip boundary conditions on the left and right boundary would be used compressional forces would create unrealistic downwellings along the left and the right boundary.

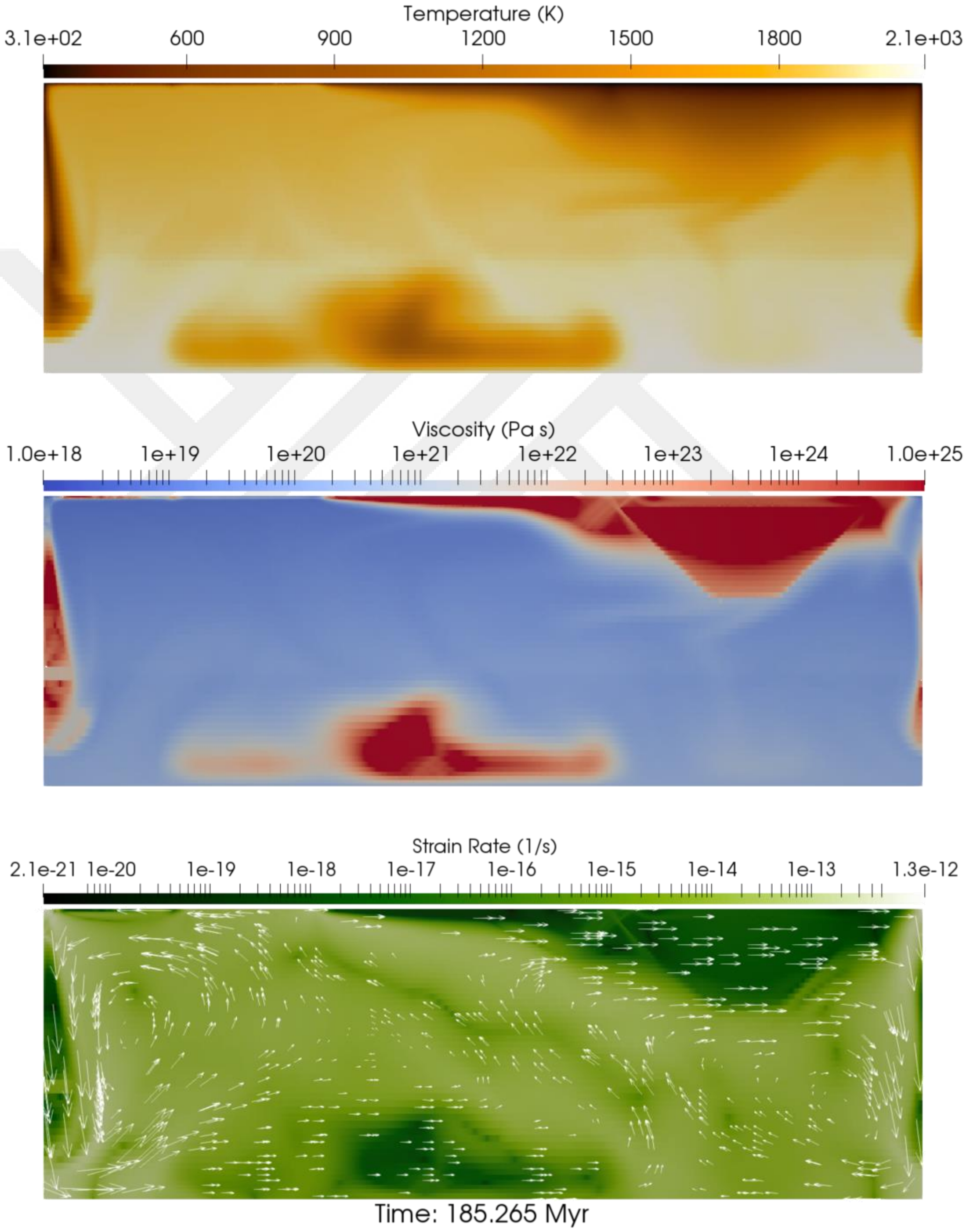

Figure 3.20 : A secondary drip forms as craton pushes the buoyant lithosphere.

3.5 Effects of Reference Mantle Viscosity (Experiment D1 & Experiment D2)

This experiment set has been conducted to investigate the effects of reference mantle viscosity. Viscosity values of 10^{19} Pa s and 10^{21} Pa s have been used for the experiments D1, and D2, respectively. This model set suggest that, increasing mantle viscosity applies higher stress on the cratonic keels, thus, making them more mobile. It has been observed that, with the increasing mantle viscosity craton starts to move much earlier from the reference model (by a factor of 20 - 30 times).

3.5.1 Experiment D1

On Experiment D1, asthenosphere viscosity is 10 times lower than the reference model. Other related model parameters used in the numerical calculations are given in Table 3.8. It has been observed that 10^{19} Pa s mantle viscosity cannot apply enough stress to mobilize the craton.

Both cratonic keel and oceanic lithosphere becomes thicker in time, because they are stable. Small-scale lithospheric drips are observed throughout the oceanic lithosphere and on the root of the craton.

As the model progresses, cratonic keel becomes wider, but thinner. Also, deformation on the oceanic lithosphere, created by the small-scale viscous drips can be observed on viscosity and strain rate profiles. As a result of deformation of the oceanic lithosphere due to drips, an undulation pattern becomes more distinctive along the oceanic lithosphere – asthenosphere boundary (Figure 3.21).

Table 3.8 : Model parameters for Experiment D1.

Experiment # D1		
Reference Mantle Viscosity	10^{19}	Pa s
Surface Yield Stress	20	MPa
Friction Coefficient	0.1	
Thermal Anomaly Size	0.5	
Eclogite Phase Transition Depth	40	km
Cohesion	10^{3}	Pa
Deformation Mechanism	Diffusion	
Continent Radius (km)	300	km
Mantle Flow Velocity	4	cm/yr
Mantle Flow Starting Depth	60	km

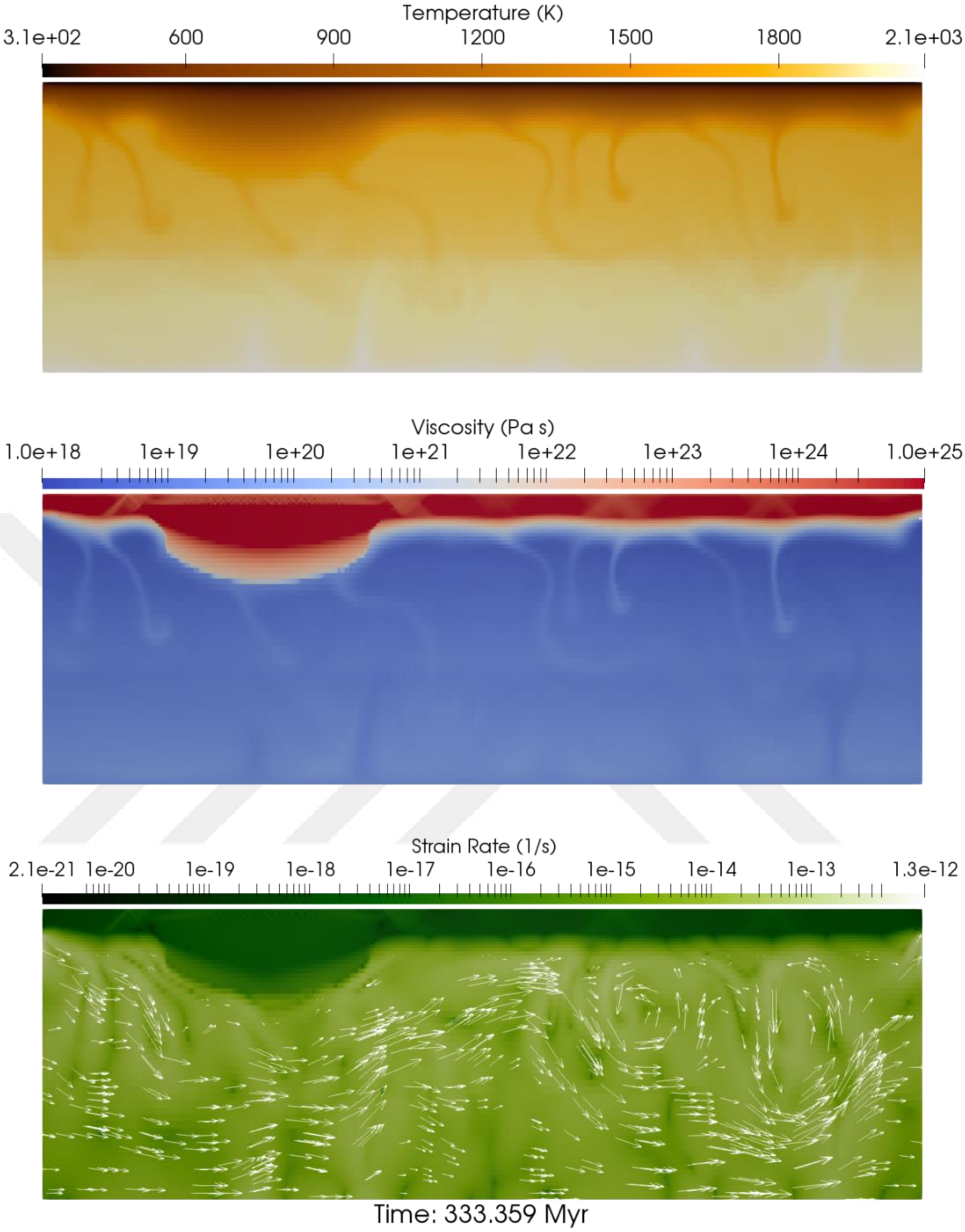

Figure 3.21 : Craton becomes wider and thinner in time, and undulation due to deformation of the oceanic lithosphere can be observed.

3.5.2 Experiment D2

In Experiment D2, reference mantle viscosity has chosen to be 10^{21} Pa s. All the other parameters are same as the reference model. Other model parameters are given in Table 3.9. Higher viscosity fluids apply higher pressure to the things they encounter. As a result, cratonic keel has become mobilized 22-23 times faster than the reference experiment. Big difference in the mobilization times reflects the importance of reference mantle viscosity in creating mantle wind-based stresses. 10 times difference in the reference mantle viscosity leads to ~20 times difference in the mobilization time.

Table 3.9 : Model Parameters for Experiment D2.

Experiment # D2		
Reference Mantle Viscosity	10^{21}	Pa s
Surface Yield Stress	20	MPa
Friction Coefficient	0.1	
Thermal Anomaly Size	0.5	
Eclogite Phase Transition Depth	40	km
Cohesion	10^{3}	Pa
Deformation Mechanism	Diffusion	
Continent Radius (km)	300	km
Mantle Flow Velocity	4	cm/yr
Mantle Flow Starting Depth	60	km

In the first 7 Myr, craton has already started to drift away. Rift imposed on the left side of the craton broadens due to asthenospheric ascend. Enlargement of the rift leads to crustal thickening, and subsequently, eclogitization. Eclogitized denser parts start to sink in forms of thin slabs. Even though oceanic lithosphere should be unsubductable due to thin oceanic mantle lithosphere and hot temperatures, denser parts pull the rest of the lithosphere into the mantle (Figure 3.22).

Sometime after, first “slab” breaks-off while a second one is forming on the rift zone. Rising asthenosphere fills the gaps caused by the downwelling of the oceanic lithosphere. Asthenospheric rocks applies force on the existing oceanic lithosphere and pulls it down as they go upwards (Figure 3.23). Another break-off takes place on the second slab, probably because of the hot mantle temperatures. Hot mantle temperature makes oceanic slab weaker. If a slab becomes weaker it is harder for it to stay intact and, on the weakest part it becomes thinner and breaks off, eventually.

Process is repeated again with the formation of new oceanic material due to cooling of asthenospheric rocks, and compression caused by the drifting continent (Figure 3.24). Sinking slabs seen in the model are purely formed due to crustal thickening. Then, it can be interpreted as; if given certain conditions are ever met in Archean, regions of crustal thickening within the oceanic lithosphere might have been driven the episodic recycling of the oceanic lithosphere into the mantle. Higher mantle temperatures in the Archean would not let the oceanic lithosphere subduct continuously like in the modern-day subduction systems. Thus, even if there was subduction it was probably episodic subduction.

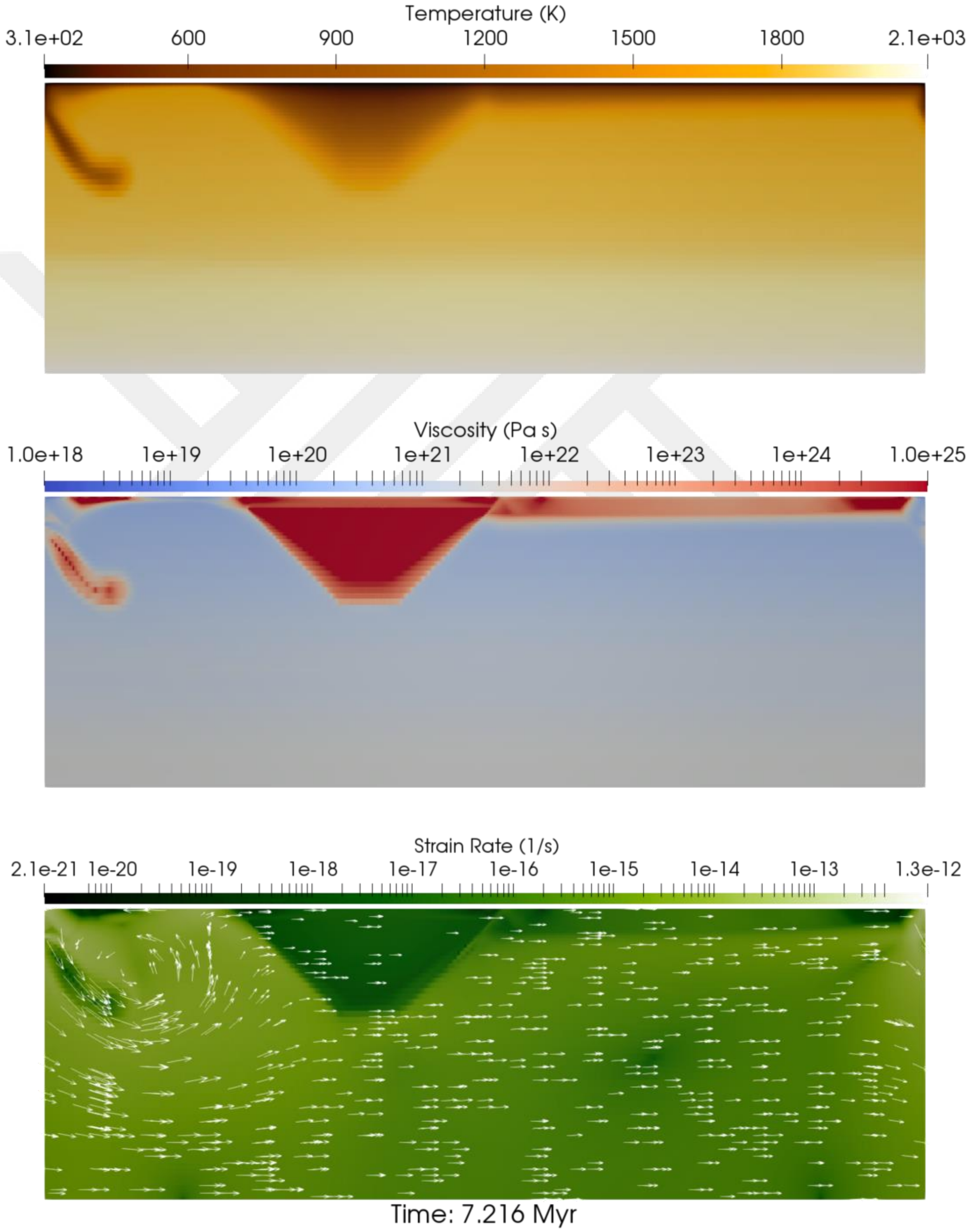

Figure 3.22 : Craton becomes mobilized at t = 7.216 Myr. Asthenosphere rising through the rift drags oceanic lithosphere into the mantle.

On models with higher reference mantle viscosity oceanic lithosphere completely detaches from the continental part. The rift implemented on the left side of the craton to provide separation of the ocis more effective when compared with the lower viscosity models, because of the faster mobilization of the craton.

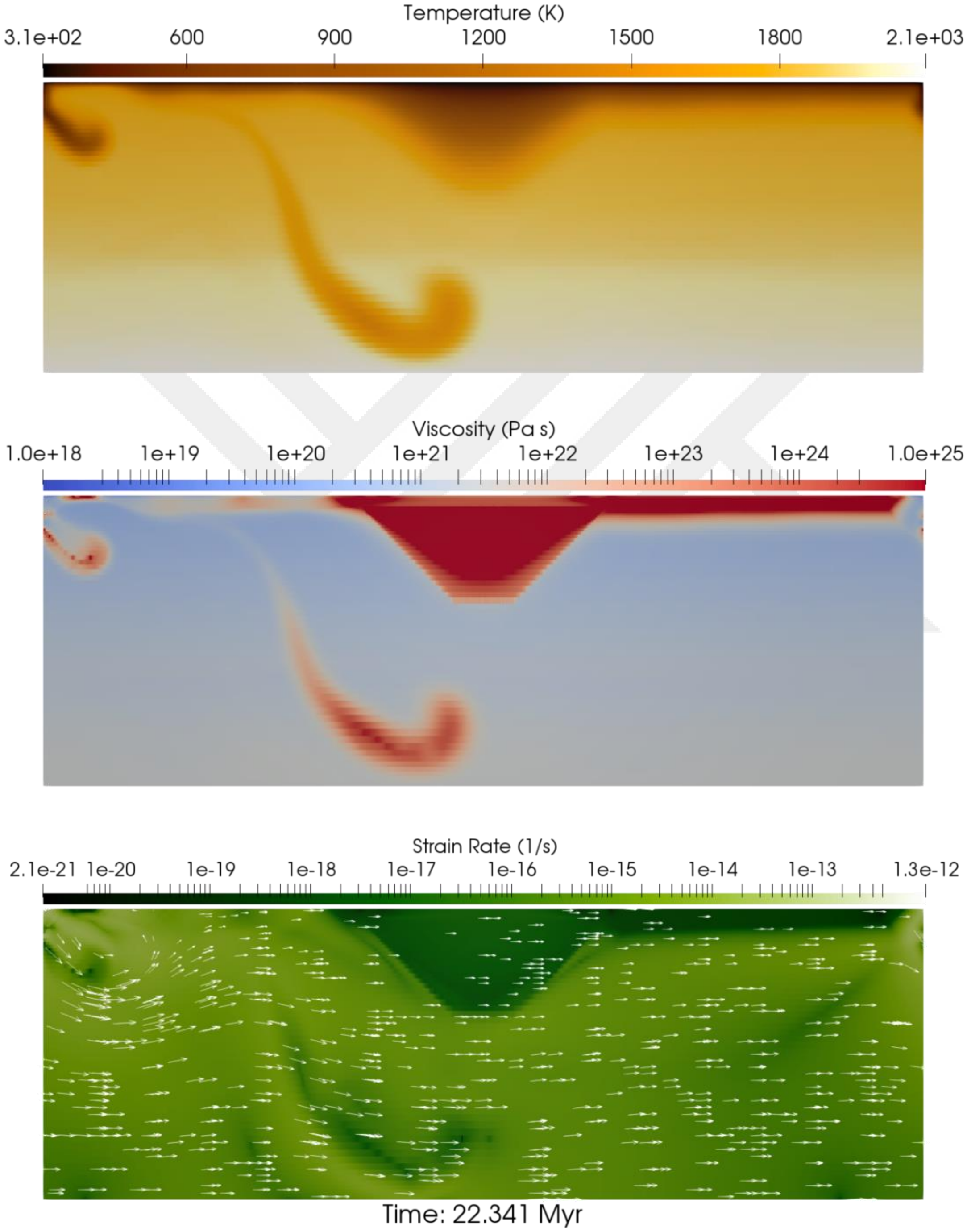

Figure 3.23 : First part of oceanic lithosphere that has been sinking breaks-off, while a second one starts to form out of newly formed oceanic crust.

Faster mobilization does not allow for mantle rocks to rise upwards to fill gaps and cool down. That way oceanic lithosphere cannot stick to the craton, instead just becomes separated and gets thicker by the upwelling asthenospheric rocks to form downgoing slabs.

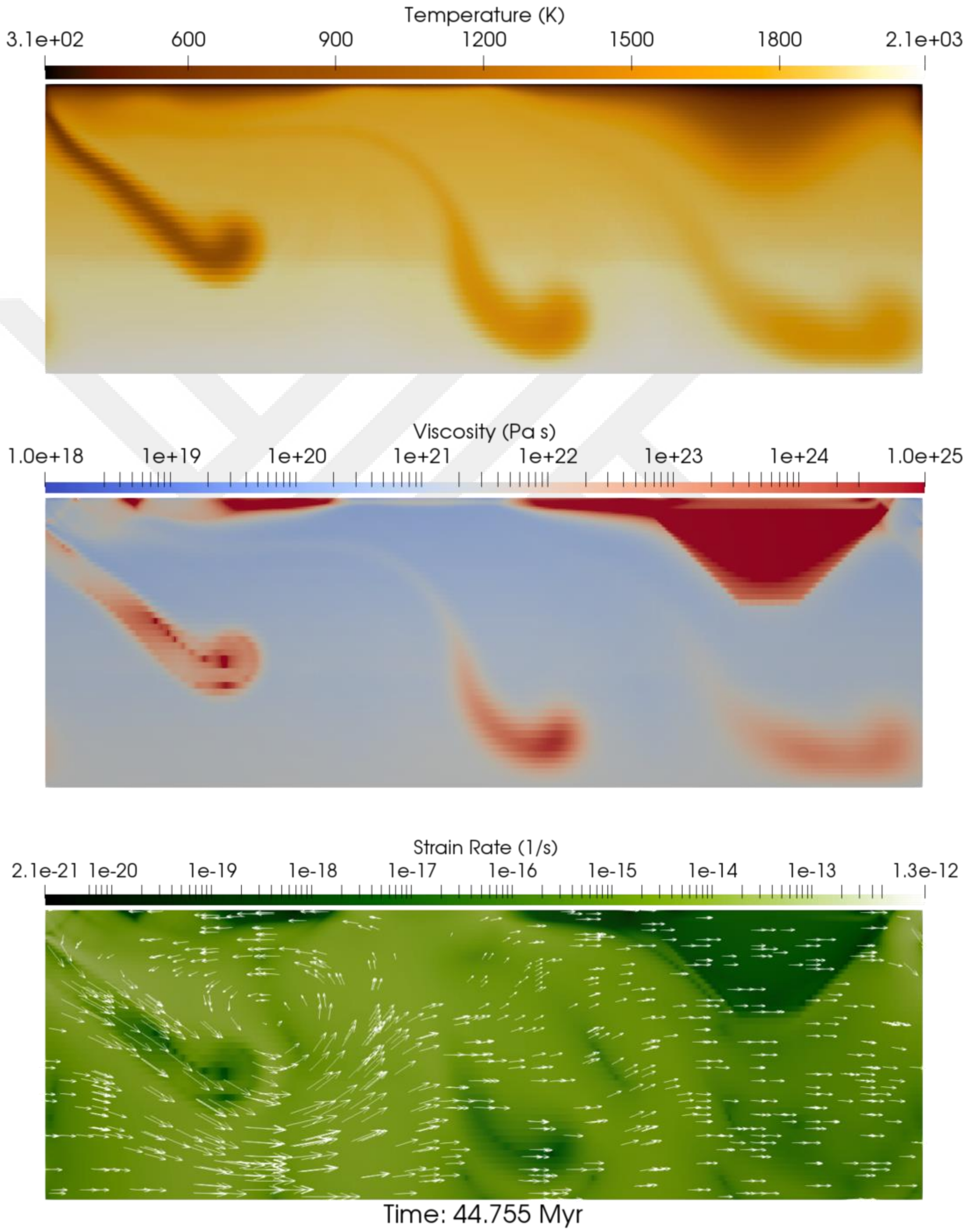

Figure 3.24 : Second slab breaks-off, a third one forms and starts to sink down as previous ones.

Migration of the craton to the right boundary from the starting position can give an idea about the movement pace of the craton. Initially, craton is 300 km wide on the surface, and its center is located at the x = 500 km, within the 2000 km wide model box. Thus, when the right side of the craton contacts the right boundary, that means that it has been drifted 1350 km away from its starting position. Migration times for each model discussed in the previous chapter is given in Figure 3.25.

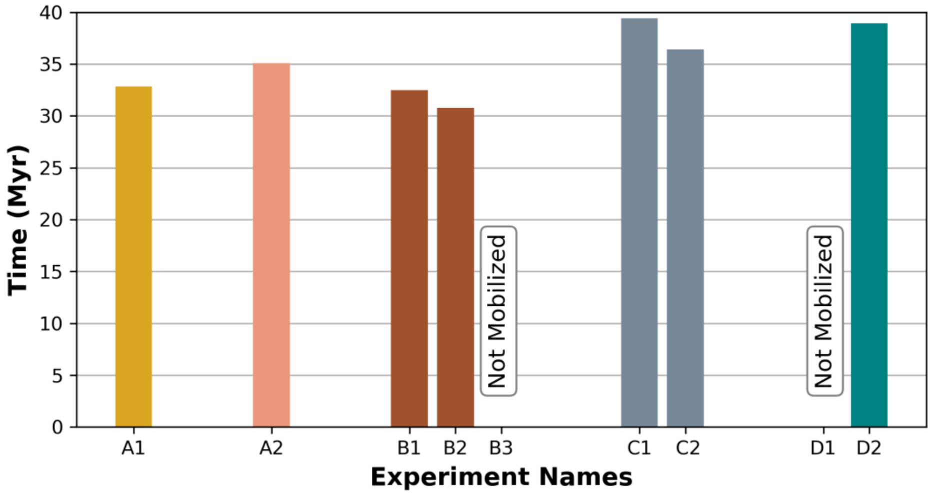

Figure 3.25 : 1350 km displacement of the cratonic roots for each model.

It takes 32 Myr for craton to reach to the right boundary in the reference model (Experiment A1). When the deformation mechanism has been changed to dislocation creep (Experiment A2), it takes 2.5 – 3 Myr longer for craton to reach a 1350 km horizontal displacement. Surface yield stress parameter, although it changes the tectonic evolution of the model thoroughly, have little to no effect on the migration time (Experiment Set B). Eclogite phase transition depth prolongs the time 4 Myr and 4.6 Myr for 50 km and 60 km, respectively (Experiment Set C). Increments in the reference mantle viscosity, increases the time needed for craton to migrate 1350 km horizontally (Experiment Set D). Even though, increasing viscosity starts to drift the craton earlier, actual time required for it to reach the right boundary takes 5-6 Myr longer than the reference model.

Diversity of the model results required a need for detailed classification. Classification of the results and corresponding experiments are given in Figure 3.26, and summarization of all model results are given in Table 3.10.

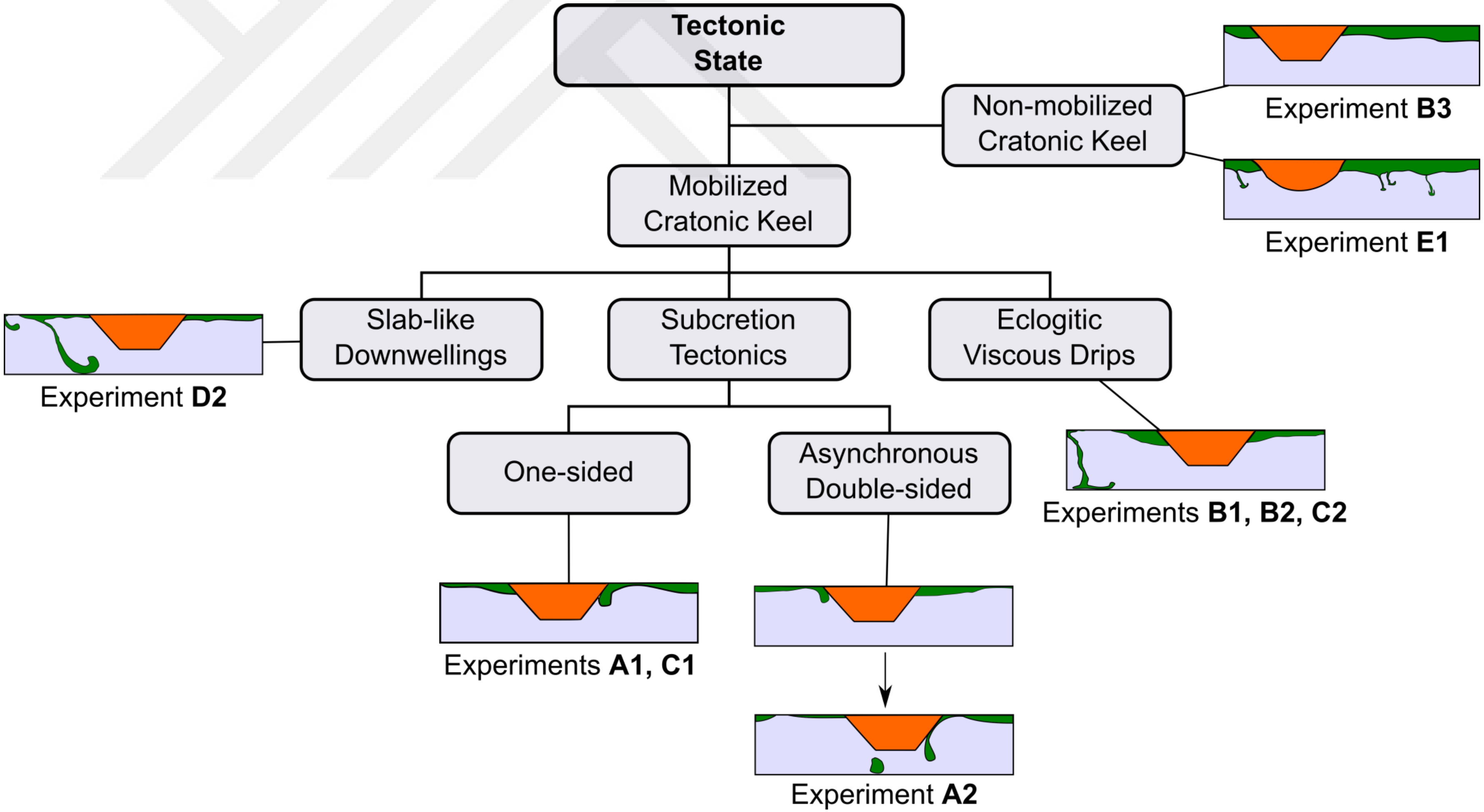
Tectonic State
Non-mobilized Cratonic Keel
Experiment **B3**
Experiment **E1**
Mobilized Cratonic Keel
Slab-like Downwellings
Subcretion Tectonics
Eclogitic Viscous Drips
Experiment **D2**
One-sided
Asynchronous Double-sided
Experiments **B1, B2, C2**
Experiments **A1, C1**
Experiment **A2**

Figure 3.26 : Classification of different behaviors observed in the study, and corresponding experiments.

Table 3.10 : Summarization of Experimental Results.

Parameter	Reference Model	Deformation Mechanism	Surface Yield Stress			Eclogite Phase Transition Depth		Reference Mantle Viscosity	
Model Name	A1	A2	B1	B2	B3	C1	C2	D1	D2
Value	-	Dislocation	25 MPa	30 MPa	40 MPa	50 km	60 km	10^{19} Pa s	10^{21} Pa s
Tectonic State	One-sided subcretion	Asynchronous double-sided subcretion	Eclogitic Drips	Eclogitic Drips	Non-mobilized cratonic keel	One-sided subcretion	Eclogitic Drips	Non-mobilized cratonic keel	Slab-like
Mobilization Time (Myr)	160.207	195.58	207.436	318.616	Non-mobilized	136.305	150.577	Non-mobilized	<7
Migration Time for Δx=1350 km (Myr)	193.063	230.687	239.938	349.395	-	175.744	186.982	-	44.955
Total Travel Time (Myr)	32.856	35.107	32.502	30.779	-	39.439	36.405	-	38.96 - 44.95

Firstly, model results classified by their tectonic state. Tectonically unstable models have been separated into three different categories by their dominant lithospheric removal mechanism: (i) slab-like downwellings, (ii) subcretion tectonics, and (iii) eclogitic viscous drips. Subcretion section divided into two sub-categories as, one-sided subcretion and asynchronous double-sided subcretion. On tectonically stable models craton does not move until the pre-imposed last time step, which corresponds to ~450 Myr. Nevertheless, this value can be longer or shorter depending on the viscosity fluctuations within the iterations. Tectonically stable models can be observed when surface yield stresses are sufficiently high or, reference mantle viscosities are low enough. When surface yield stress is high enough to stop the movement of the craton, oceanic lithosphere thickens along the model box (Experiment B3). Furthermore, if reference mantle viscosity is low enough, small-scaled viscous drips forms beneath the oceanic lithosphere while craton undergoes rounding by thermal erosion due to low viscosity, vigorous mantle winds.

4. CONCLUSIONS

Mantle flows created by mantle overturns can mobilize pre-existing cratons under Archean conditions, yet, mobilization of cratons does not always end up with subcretion. Our numerical experiments show that, main driving forces determining the tectonic regime in such settings are; reference mantle viscosity, surface yield stress and eclogite phase transition depth.

Stress applied by the mantle winds on the cratonic keel is the main driving force behind the mobilization of a craton. Higher viscosities apply higher stresses on cratonic keel; hence, drifting starts much earlier. Experiments showed that, when asthenospheric viscosity is higher (i.e. 10^{21} Pa s or 10^{22} Pa s), it mobilizes the craton approximately by a factor of twenty compared with the reference experiment, where mantle viscosity has chosen to be 10^{20}.

Reference mantle viscosity affects the geodynamic regime drastically. When a viscosity value of 10^{19} Pa s used, cratonic keel did not drift away probably due to insufficient stress generation. Nonetheless, mantle convections that are relatively small wavelength become more vigorous with decreasing viscosities and thermally erodes the cratonic roots, and base of the oceanic lithosphere. In contrast, when mantle viscosity is 10^{21} Pa s recycling of the oceanic lithosphere takes form of slab-like features that resemble to modern-day subducting plates. This change in the geodynamic regime, depending on the mantle viscosity, can be analogous to change in the tectonic regime that comes with cooling of the Earth (from stagnant-lid to plate tectonics) (Figure 4.1).

Increasing yield stress makes oceanic lithosphere stronger and changes the style of deformation. When yield stress of 30 MPa used in the Experiment 11, cratonic drifting did not started until ~300 Myr, which is ~150 Myr longer from the measured time in the reference model. Furthermore, when it was raised to 40 MPa, craton did not move until the last time step (476 Myr). The critical depth of phase transition from basalt to eclogite, extends the times of cratonic migration around 4-5 Myr.

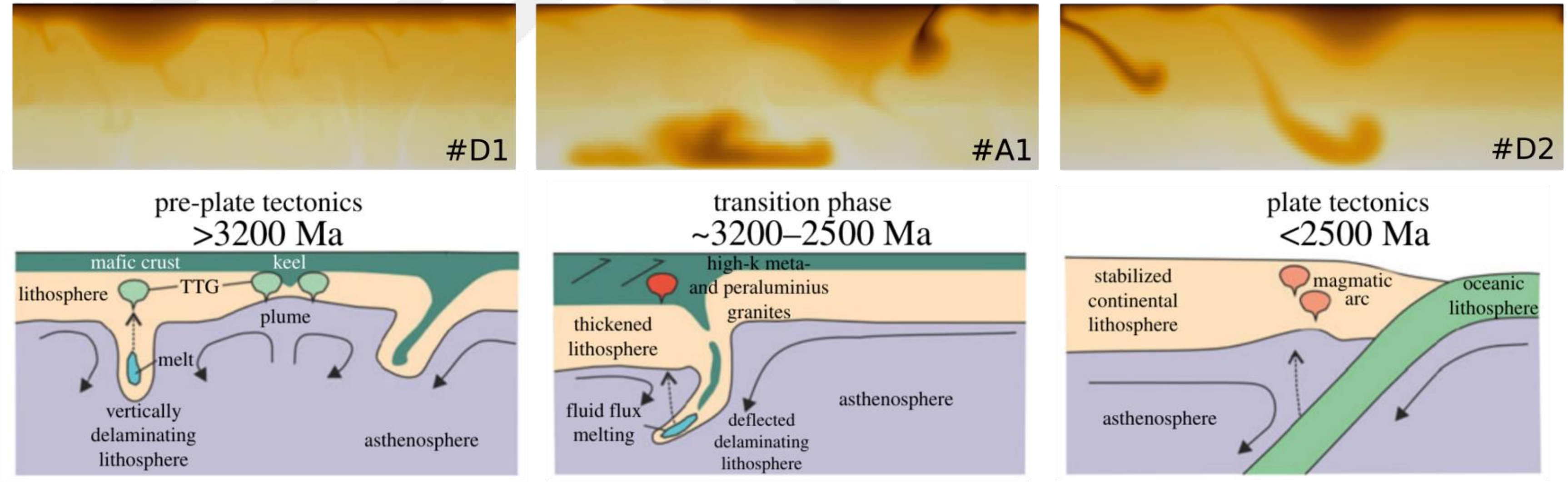
#D1
#A1
#D2
pre-plate tectonics
>3200 Ma
mafic crust
keel
lithosphere
TTG
plume
melt
vertically
delaminating
lithosphere
asthenosphere
transition phase
~3200–2500 Ma
high-k meta-
and peraluminius
granites
thickened
lithosphere
fluid flux
melting
deflected
delaminating
lithosphere
asthenosphere
plate tectonics
<2500 Ma
stabilized
continental
lithosphere
magmatic
arc
oceanic
lithosphere
asthenosphere

Figure 4.1 : Comparison of different experiments with varying viscosities from this study and evolution of tectonic regime in the Archean according to Cawood et al. (2018).

Both of the experiments with a deeper eclogite transition depth (Experiment C1 and Experiment C2) moves backwards at some point within the model due to direction convection cells. Backwards movement and/or stalling of craton throughout the experiment have also been observed on Reference Experiment A1, Experiment A2 and Experiment D2 due to same reason.

On Experiment A2, dislocation creep has been chosen as the main deformation mechanism instead of diffusion creep which leads mobilization time to become longer (i.e. the craton starts to drift away at t = 195.580 Myr). Convection cells formed by the deformation occurred on the oceanic lithosphere, starts to push the craton backwards for around 5 Myr, starting at t = 205.981 Myr. Inverted movement direction of the craton results in subcretion of the oceanic lithosphere on the left margin. Afterwards, craton starts to move through right boundary as the forces applied by the convection cells fade away. This cause a secondary subcretion formed on the right side of the craton, leading to asynchronous double-sided subcretion.

Experimental results showed that, lithospheric removal mechanisms and craton mobilization times can vary with different parameters, but a displacement of 1350 km takes place in 30 to 40 Myr when the craton becomes mobile. Subcretion tectonics can only start in a narrow window, where surface yield stress is 20 MPa and reference mantle viscosity is 10^{20} Pa s, with the exception of eclogite transition depth being 60 km. Results indicate that subcretion mechanism can be achieved under given conditions, and TTG genesis via this mechanism can be valid when certain P-T conditions are met.

REFERENCES

Arndt, N. T., Coltice, N., Helmstaedt, H., & Gregoire, M. (2009). Origin of Archean subcontinental lithospheric mantle: Some petrological constraints. *Lithos*, *109*(1–2), 61–71. https://doi.org/10.1016/j.lithos.2008.10.019.

Arndt, Nicholas T. (2013). Section 5. Generation of TTG and Archean Tectonics. *Geochemical Perspectives*, *2*(3), 436–462. Retrieved from http://perspectives.geoscienceworld.org/content/2/3/436.short.

Artemieva, I. (2011). The lithosphere: An interdisciplinary approach. In *The Lithosphere: An Interdisciplinary Approach*. https://doi.org/10.1017/CBO9780511975417.

Aulbach, S., Stachel, T., Heaman, L. M., Creaser, R. A., & Shirey, S. B. (2011). Formation of cratonic subcontinental lithospheric mantle and complementary komatiite from hybrid plume sources. *Contributions to Mineralogy and Petrology*, *161*(6), 947–960. https://doi.org/10.1007/s00410-010-0573-4.

Bédard, J. H. (2006). A catalytic delamination-driven model for coupled genesis of Archaean crust and sub-continental lithospheric mantle. *Geochimica et Cosmochimica Acta*, *70*(5), 1188–1214. https://doi.org/10.1016/j.gca.2005.11.008.

Bédard, J. H. (2018). Stagnant lids and mantle overturns: Implications for Archaean tectonics, magmagenesis, crustal growth, mantle evolution, and the start of plate tectonics. *Geoscience Frontiers*, *9*(1), 19–49. https://doi.org/10.1016/j.gsf.2017.01.005.

Bédard, J. H., Brouillette, P., Madore, L., & Berclaz, A. (2003). Archaean cratonization and deformation in the northern Superior Province, Canada: An evaluation of plate tectonic versus vertical tectonic models. *Precambrian Research*. https://doi.org/10.1016/S0301-9268(03)00181-5.

Breuer, D. (2011). Stagnant Lid Convection. In M. Gargaud, R. Amils, J. C. Quintanilla, H. J. (Jim) Cleaves, W. M. Irvine, D. L. Pinti, & M. Viso (Eds.), *Encyclopedia of Astrobiology* (p. 1569). https://doi.org/10.1007/978-3-642-11274-4_1499.

Brown, M. (2007). Metamorphic Conditions in Orogenic Belts: A Record of Secular Change. *International Geology Review*. https://doi.org/10.2747/0020-6814.49.3.193.

Cawood, P. A., Hawkesworth, C. J., Pisarevsky, S. A., Dhuime, B., Capitanio, F. A., & Nebel, O. (2018). Geological archive of the onset of plate tectonics. *Philosophical Transactions of the Royal Society A: Mathematical, Physical and Engineering Sciences*. https://doi.org/10.1098/rsta.2017.0405.

Cawood, P. A., Kröner, A., & Pisarevsky, S. (2006). Precambrian plate tectonics: Criteria and evidence. *GSA Today*. https://doi.org/10.1130/GSAT01607.1.

Condie, K. C., Aster, R. C., & Van Hunen, J. (2016). A great thermal divergence in the mantle beginning 2.5 Ga: Geochemical constraints from greenstone basalts and komatiites. *Geoscience Frontiers*. https://doi.org/10.1016/j.gsf.2016.01.006.

Condie, K. C., & Benn, K. (2013). Archean Geodynamics: Similar to or Different from Modern Geodynamics? In *Archean Geodynamics and Environments*. https://doi.org/10.1029/164GM05.

Condie, K. C., & Kröner, A. (2008). When did plate tectonics begin? Evidence from the geologic record. In *Special Paper 440: When Did Plate Tectonics Begin on Planet Earth?* https://doi.org/10.1130/2008.2440(14).

Cooper, C. M., Lenardic, A., Levander, A., & Moresi, L. (2006). Creation and preservation of cratonic lithosphere: Seismic constraints and geodynamic models. *Geophysical Monograph Series*, *164*(July 2015), 75–88. https://doi.org/10.1029/164GM07.

Fischer, R., & Gerya, T. (2016). Early Earth plume-lid tectonics: A high-resolution 3D numerical modelling approach. *Journal of Geodynamics*. https://doi.org/10.1016/j.jog.2016.03.004.

Gerya, T. (2014). Precambrian geodynamics: Concepts and models. *Gondwana Research*, *25*(2), 442–463. https://doi.org/10.1016/j.gr.2012.11.008.

Gray, R., & Pysklywec, R. N. (2012). Geodynamic models of mature continental collision: Evolution of an orogen from lithospheric subduction to continental retreat/delamination. *Journal of Geophysical Research: Solid Earth*, *117*(3), 1–14. https://doi.org/10.1029/2011JB008692.

Griffin, W. L., O'Reilly, S. Y., Afonso, J. C., & Begg, G. C. (2009). The Composition and Evolution of Lithospheric Mantle: a Re-evaluation and its Tectonic Implications. *Journal of Petrology*, *50*(7), 1185–1204. https://doi.org/10.1093/petrology/egn033.

Groves, D. I., Ho, S. E., Rock, N. M. S., Barley, M. E., & Muggeridge, M. T. (1987). Archean cratons, diamond and platinum: Evidence for coupled long-lived crust-mantle systems. *Geology*, *15*(9), 801. https://doi.org/10.1130/0091-7613(1987)15<801:ACDAPE>2.0.CO;2.

Hacker, B. R. (1996). Eclogite formation and the rheology, buoyancy, seismicity, and H2O content of oceanic crust. In *Geophysical Monograph Series*. https://doi.org/10.1029/GM096p0337.

Hamilton, W. B. (1998). Archean magmatism and deformation were not products of plate tectonics. *Precambrian Research*. https://doi.org/10.1016/S0301-9268(98)00042-4.

Hamilton, W. B. (2011). Plate tectonics began in Neoproterozoic time, and plumes from deep mantle have never operated. *Lithos*. https://doi.org/10.1016/j.lithos.2010.12.007.

Harrison, T. M., Schmitt, A. K., McCulloch, M. T., & Lovera, O. M. (2008). Early (≥ 4.5 Ga) formation of terrestrial crust: Lu-Hf, δ18O, and Ti thermometry results for Hadean zircons. *Earth and Planetary Science Letters*. https://doi.org/10.1016/j.epsl.2008.02.011.

Hastie, A. R., & Fitton, J. G. (2019). Eoarchaean tectonics: New constraints from high pressure-temperature experiments and mass balance modelling. *Precambrian Research*. https://doi.org/10.1016/j.precamres.2019.02.006.

Herzberg, C., Condie, K., & Korenaga, J. (2010). Thermal history of the Earth and its petrological expression. *Earth and Planetary Science Letters*. https://doi.org/10.1016/j.epsl.2010.01.022.

Johnson, T. E., Brown, M., Kaus, B. J. P., & Vantongeren, J. A. (2014). Delamination and recycling of archaean crust caused by gravitational instabilities. *Nature Geoscience*, *7*(1), 47–52. https://doi.org/10.1038/ngeo2019.

Jordan, T. H. (1978). Composition and development of the continental tectosphere. *Nature*. https://doi.org/10.1038/274544a0.

Kelemen, P. B., Hart, S. R., & Bernstein, S. (1998). Silica enrichment in the continental upper mantle via melt/rock reaction. *Earth and Planetary Science Letters*. https://doi.org/10.1016/S0012-821X(98)00233-7.

King, S. D. (2005). Archean cratons and mantle dynamics. *Earth and Planetary Science Letters*, *234*(1–2), 1–14. https://doi.org/10.1016/j.epsl.2005.03.007.

Lee, C. T. A. (2006). Geochemical/petrologic constraints on the origin of cratonic mantle. In *Geophysical Monograph Series*. https://doi.org/10.1029/164GM08.

Lenardic, A., & Moresi, L.-N. (1999). Some thoughts on the stability of cratonic lithosphere: Effects of buoyancy and viscosity. *Journal of Geophysical Research: Solid Earth*, *104*(B6), 12747–12758. https://doi.org/10.1029/1999JB900035.

Lourenço, D. L., Rozel, A., & Tackley, P. J. (2016). Melting-induced crustal production helps plate tectonics on Earth-like planets. *Earth and Planetary Science Letters*, *439*, 18–28. https://doi.org/10.1016/j.epsl.2016.01.024.

Martin, H. (1987). Petrogenesis of archaean trondhjemites, tonalites, and granodiorites from Eastern Finland: Major and trace element geochemistry. *Journal of Petrology*. https://doi.org/10.1093/petrology/28.5.921.

Moore, W. B., & Webb, A. A. G. (2013). Heat-pipe earth. *Nature*, *501*(7468), 501–505. https://doi.org/10.1038/nature12473.

Moyen, J. F., & Martin, H. (2012). Forty years of TTG research. *Lithos*, *148*, 312–336. https://doi.org/10.1016/j.lithos.2012.06.010.

Moyen, J. F., Stevens, G., Kisters, A. F. M., & Belcher, R. W. (2007). Chapter 5.6 TTG Plutons of the Barberton Granitoid-Greenstone Terrain, South Africa. *Developments in Precambrian Geology*. https://doi.org/10.1016/S0166-2635(07)15056-8.

O'Neill, C., & Roberts, N. M. W. (2018). Lid tectonics – Preface. *Geoscience Frontiers*. https://doi.org/10.1016/j.gsf.2017.10.004.

Polat, A. (2012). Growth of Archean continental crust in oceanic island arcs. *Geology*. https://doi.org/10.1130/focus042012.1.

Rolf, T., & Tackley, P. J. (2011). Focussing of stress by continents in 3D spherical mantle convection with self-consistent plate tectonics. *Geophysical Research Letters*. https://doi.org/10.1029/2011GL048677.

Rollinson, H. (2010). Coupled evolution of Archean continental crust and subcontinental lithospheric mantle. *Geology*. https://doi.org/10.1130/G31159.1.

Rozel, A. B., Golabek, G. J., Jain, C., Tackley, P. J., & Gerya, T. (2017). Continental crust formation on early Earth controlled by intrusive magmatism. *Nature*, *545*(7654), 332–335. https://doi.org/10.1038/nature22042.

Schulze, D. J. (1989). Constraints on the abundance of eclogite in the upper mantle. *Journal of Geophysical Research*. https://doi.org/10.1029/JB094iB04p04205.

Shirey, S. B., Richardson, S. H., & Harris, J. W. (2004). Integrated models of diamond formation and craton evolution. *Lithos*, *77*(1–4), 923–944. https://doi.org/10.1016/J.LITHOS.2004.04.018.

Sizova, E., Gerya, T., Stüwe, K., & Brown, M. (2015). Generation of felsic crust in the Archean: A geodynamic modeling perspective. *Precambrian Research*, *271*, 198–224. https://doi.org/10.1016/j.precamres.2015.10.005.

Smithies, R. H., Van Kranendonk, M. J., & Champion, D. C. (2007). The Mesoarchean emergence of modern-style subduction. *Gondwana Research*. https://doi.org/10.1016/j.gr.2006.02.001.

Smithies, R. Hugh, Champion, D. C., Van Kranendonk, M. J., Howard, H. M., & Hickman, A. H. (2005). Modern-style subduction processes in the Mesoarchaean: Geochemical evidence from the 3.12 Ga Whundo intra-oceanic arc. *Earth and Planetary Science Letters*. https://doi.org/10.1016/j.epsl.2004.12.026.

Stern, R. J. (2008). Modern-style plate tectonics began in Neoproterozoic time: An alternative interpretation of Earth's tectonic history. In *Special Paper 440: When Did Plate Tectonics Begin on Planet Earth?* https://doi.org/10.1130/2008.2440(13).

Stern, R. J. (2018). The evolution of plate tectonics Subject Areas : Author for correspondence : *Philosophical Transactions of the Royal Society A: Mathematical, Physical and Engineering Sciences*, *376*(2132). https://doi.org/10.1098/rsta.2017.0406.

Tackley, P. J. (2008). Modelling compressible mantle convection with large viscosity contrasts in a three-dimensional spherical shell using the yin-yang grid. *Physics of the Earth and Planetary Interiors*, *171*(1–4), 7–18. https://doi.org/10.1016/j.pepi.2008.08.005.

Ueda, K., Gerya, T., & Sobolev, S. V. (2008). Subduction initiation by thermal-chemical plumes: Numerical studies. *Physics of the Earth and Planetary Interiors*. https://doi.org/10.1016/j.pepi.2008.06.032.

van Hunen, J., & Moyen, J.-F. (2012). Archean Subduction: Fact or Fiction? *Annual Review of Earth and Planetary Sciences*. https://doi.org/10.1146/annurev-earth-042711-105255.

Van Kranendonk, Martin J. (2007). Chapter 7.2 A Review of the Evidence for Putative Paleoarchean Life in the Pilbara Craton, Western Australia. *Developments in Precambrian Geology*. https://doi.org/10.1016/S0166-2635(07)15072-6.

Van Kranendonk, Martin J. (2011). Onset of plate tectonics. *Science*. https://doi.org/10.1126/science.1208766.

Van Kranendonk, Martin Julian. (2011). Archean Tectonics. In M. Gargaud, R. Amils, J. C. Quintanilla, H. J. (Jim) Cleaves, W. M. Irvine, D. L. Pinti, & M. Viso (Eds.), *Encyclopedia of Astrobiology* (pp. 69–74). https://doi.org/10.1007/978-3-642-11274-4_100.

Wen, L., & Anderson, D. L. (1997). Slabs, hotspots, cratons and mantle convection revealed from residual seismic tomography in the upper mantle. *Physics of the Earth and Planetary Interiors*, *99*(1–2), 131–143. https://doi.org/10.1016/S0031-9201(96)03162-7.

Zegers T.E., van K. P. E. (2001). Middle Archean continent formation by crustal delamination. *Geology*. https://doi.org/10.1130/0091-7613(2001)029<1083:MACFBC>2.0.CO;2.

CURRICULUM VITAE

Name Surname : Uğurcan ÇETİNER

Place and Date of Birth : Tekirdağ-Turkey / 03.06.1994

E-Mail : cetineru@itu.edu.tr

EDUCATION :

- **B.Sc.** : 2017, Istanbul Technical University, Faculty of Mines, Mineral Processing Engineering
- **M.Sc.** : 2019, Istanbul Technical University, Eurasia Institute of Earth Sciences